Structural, optical and sensing properties of cobalt and indium doped zinc oxide prepared mechano-chemically

by

Mahlatse Fortunate Manamela

A dissertation submitted in partial fulfilment of the requirements for the degree of Master of Science in Physics in the Department of Physics, School of Physical and Mineral Sciences, Faculty of Science and Agriculture, University of Limpopo, RSA

Supervisor: Prof TE Mosuang

Co-supervisor: Dr BW Mwakikunga

Declaration

I declare that the work reported under the title “Structural, optical and sensing properties of cobalt and indium doped zinc oxide prepared mechano-chemically” submitted to the University of Limpopo for the fulfilment of a Master of Science degree in Physics is my own work that all the sources that I have used or quoted have been indicated and acknowledged by means of complete references and that this work has not been submitted before for any other degree at any other institution.

_____ _____.

Manamela M.F (Ms) **Date**

Acknowledgements

I would like to thank:

- My supervisors, Dr T. E Mosuang and Dr B. W Mwakikunga for their exclusive guidance and support for the success of this research. I would like to thank all my colleges and friends at the University of Limpopo for the sufficient input.
- I acknowledge the National Research Foundation (NRF) for their financial assistance throughout during my research.
- The Council for Scientific and Industrial Research (CSIR) branch of National Centre for Nano-structured Materials for giving access to use their equipment's.
- I am grateful to my family for being there for me, their constant support and encouragements.

Dedications

This work is dedicated to:

My mother

Phuthego Floriah Manamela

My daughter

Potego Precious Manamela

My partner

Franciscas Maropeng Komape

Abstract

The mechano-chemical technique was employed to synthesise the undoped, cobalt and indium single and double doped ZnO nanoparticles powder samples. The x-ray diffraction (XRD), scanning electron microscopy (SEM), raman spectroscopy (RS), ultraviolet-visible spectroscopy (UV-vis), and photoluminescence (PL) spectroscopy were employed to characterise the prepared samples. The XRD and energy dispersive spectroscopy (EDS) results confirmed that the prepared samples were of hexagonal wurzite form. In addition, it was found that the diffraction pattern for In-ZnO nanoparticles display an additional peak which was associated with In^{3+} dopant. The peak suggest that In^{3+} ions prefer the interstitial site in the hexagonal ZnO structure. Doping the ZnO nanoparticles with Co and In did not significantly affect the lattice parameters but the average grain sizes of the nanoparticles were found to be reduced. The morphology of the samples revealed by the SEM images appear to be more spherical. The Raman modes obtained from the excitations wavelength of 514.532 nm further indicated that the prepared samples were of hexagonal ZnO structures. The energy band gap of the prepared samples were calculated from the UV-vis data which showed that the doped ZnO nanoparticles had smaller energy band gap compared to the undoped ZnO nanoparticles. The excitation wavelength of 350 nm were used in the PL study where various defects related emissions were observed for the doped and undoped ZnO nanoparticles. The kenosistec station equipment was used to investigate the prepared samples for gas sensing application. Ammonia (NH_3), methane (CH_4) and hydrogen sulphide (H_2S) gases were probed. In all the response curves observed, the undoped and double doped ZnO nanoparticles are being favoured at a temperature range 200 – 350^oC. In addition, the double doped ZnO nanoparticles was found to be more sensitive to CH_4 at low temperatures and low

concentrations.

Table of Contents

List of figures

List of tables

Chapter 1

General Introduction

1.1 Introduction

Zinc oxide (ZnO) which is the 25th most abundant element in nature has drawn the attention of many researchers through its fascinating properties. It is a non-toxic material, highly transparent, chemically stable and is less expensive compared to other materials [1]. ZnO is formed when metallic zinc is exposed to air and forms a protective coating that protect the rest of the metal. ZnO has the three well known structural polymorphs: wurtzite (hexagonal, WZ), zincblende (cubic, ZB), and rocksalt (cubic, RS) of which among all, the wurtzite phase has received outstanding attention because it has the highest thermodynamic stability and can be synthesised easily compared to the pristine RS and ZB metastable phases [2]. Figure 1.1 shows the typical structural polymorphs of ZnO [3]. This ZnO phases have the band gap ranging between 3.27 eV (WZ) and 3.19 eV (ZB) [4], which is suitable for ultra-violet (UV) light activity only [5]. The unit cell for WZ structure has the lattice parameters being a = b = 3.250 Å and c = 5.206 Å [6].

It is an inorganic n-type semiconducting material which exhibit 60 meV for exciting binding energy at room temperature and that gives ZnO remarkable advantage in photoelectronic applications [7]. At present, ZnO is used at electronic industries as a varistor ceramic, used as an additive in rubber, and cream lotions to protect against sunburn in cosmetic industries [8]. This material is proposed for many applications in different fields of science and technology such as catalysis, sensory, photocatalytic field emission devices and solar cells [9].

Bulk and ZnO nanoparticles are very sensitive to toxic gases which are dependent on the size and morphology of sensing materials. Like, the morphology in the short nanorod indicates higher antibacterial activities compared to long nanorod and nanoplate morphologies [10]. Similarly, the nanorod-shaped particles, flat-like hexagonal shape of ZnO structures display more than fivefold increase in the photocatalytic activity for the degradation of methylene blue [11]. It is also regarded as the most efficient material in demonstrating the high efficient gas sensors for its sensitivity to gases like NH_3, O_3, NO_2, ethanol and other species [12]. Nanomaterials can appear in any nanostructure form such as nanotubes, nanowires, nanorings, nano-tetrapod and nanoparticles that allow gas molecules to diffuse into and out of the film easy [13]. These ZnO nanoparticles can be synthesised either under physical or chemical methods [14]. The physical methods include vapor condensation method [15], spray pyrolysis [16], and ball milling technique [17] while the chemical methods are thermal evaporation [18], hydrothermal processes [19], or sol-gel [20]. The method of preparation together with composition, annealing temperature and the rate of decomposition display a principal factors affecting the structural, optical and electrical properties of films and nanoparticles [21]. The advantages of using the ball milling technique is that large quantities can be produced and a wide range of different classes of materials can be obtained within speculated time [17, 22].

Transition metal (TM) oxides; SnO_2, ZnO, TiO_2, WO_2 and Ga_2O_3 are some of the oxide materials which have been examined for monitoring industrial processes and for gas sensing applications [23]. Literature has reported that tin oxide (SnO_2) and zinc oxide (ZnO) reveals higher sensitivity over a range of organic vapors and their surface area also increase when combinational sensors are incorporated by different dopants such as Co, Cu, Fe, Cr, Al, Mg, P, S, Mn at various concentrations [24]. Single and double

doping of the preferred material is possible depending on the desirable application. Extensive studies confirmed that dopants can be able to improve the reduction of grain size while the surface area of ZnO is stabilized [25]. Doping transition metals into ZnO structures are good candidate for enhancing the optical and electrical properties and were also found fascinating when observed from ferromagnetism point of view [26], [27]. In the present work ZnO nanoparticles is prepared through high energy ball milling mechano-chemical method, since it's easy to follow and operate the machine.

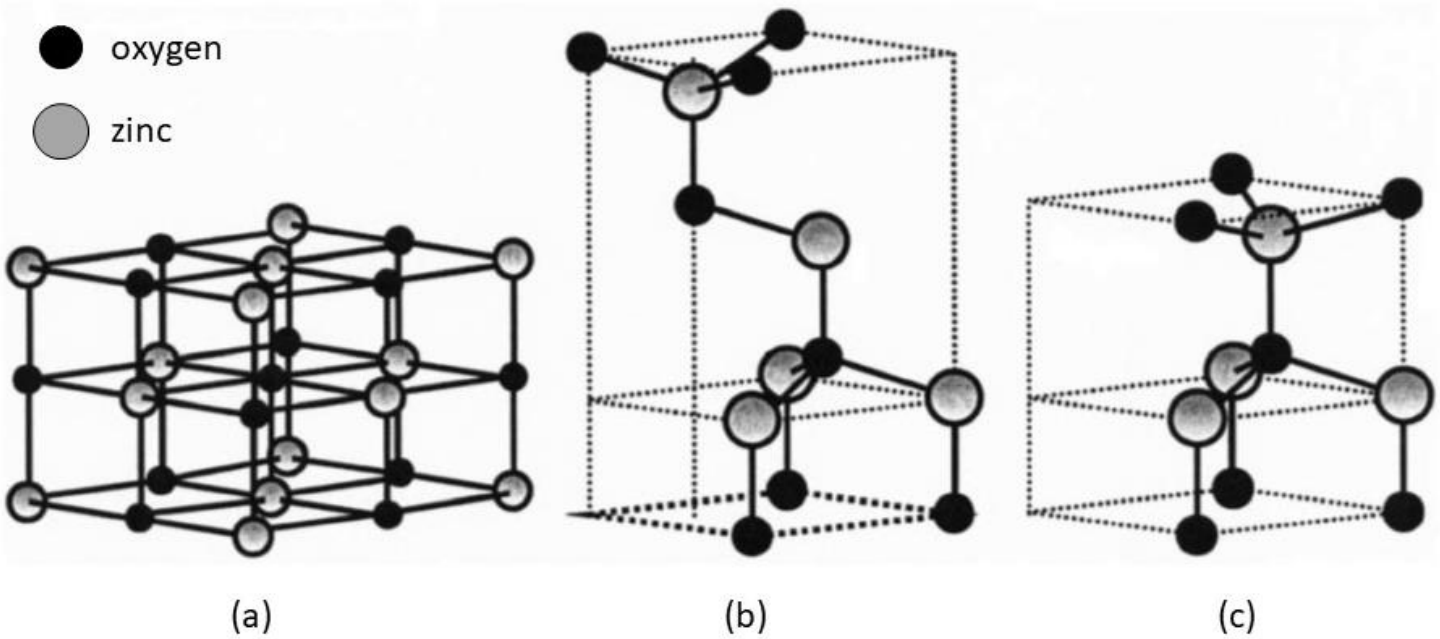

Figure 1. 1: (a) Rocksalt (b) Zinc blende (c) Wurtzite [3].

1.2 Aim and objectives

1.2.1 Aims

The aim of the study is to determine the effect of Co and In as combinational dopants on the structural, optical and sensing properties of ZnO nanoparticle powder samples synthesised mechano-chemically.

1.2.2 Objectives

The objectives of the study is to:

i. synthesise ZnO nanoparticles simultaneously doped with two metals (Co and In) mechano-chemically using ball milling,

ii. determine the structural properties of the undoped and doped ZnO nanoparticles using X-ray diffraction (XRD) and Scanning Electron Microscopy (SEM),

iii. determine optical properties of the undoped and doped ZnO nanoparticles using Raman Spectroscopy (RS), Photoluminescence (PL) and Ultraviolet-visible (UV-vis) spectroscopy,

iv. determine the effect of nano-sized pure, single doped and double doped ZnO as gas sensors.

Chapter 2

Literature review

2.1 Structural properties of ZnO

Over the past decade a great interest in semiconducting metal oxides (SMOs) has developed drastically because of their diverse properties. Especially, when SMOs particles are in their nanometer range, they display an ernomous change in their optical and magnetic properties [28]. SMOs can be obtained in different forms such as the bulk and single crystals, nanoparticles, thick and thin films materials [29]. The interesting thing about the SMOs is that they can appear in different phases depending on the kind of experimental technique followed when preparing a particular material. Various techniques are employed to control the shape, size, distribution and morphology of these oxides. ZnO nanoparticles is one of the SMOs species identified to be photosensitive, highly reactive and strong oxidizing agents, hence is a good material for photocatalytic processess [30, 31]. Ti_2O has a durable stability against photocorrosion and chemical corrosion. Now, because of this unusual optical and electronic properties of Ti_2O it makes it possible to be used in the photoelectric conversion and photocatalytic reaction [32].

Chemical methods have great achievement in controlling morphology and crystillite size than physical methods. Now, bulk and nanoparticles are obtained through techniques such as sol-gel [33], hydrothermal [34], ball milling [35] and physical vapour deposition methods [36], while the thin and thick films are synthesised using spray pyrolysis technique (SPT) [37], and chemical vapour deposition methods [38], just to name a few. Sol-gel method is easy to control, inexpensive and require low fabricating temperature which makes it an attractive method of preparing nanoparticles. Pechini's

method [33] is one of the sol-gel methods which in comparison with others yields better compositional homogeneity, lower cost and toxicity. The hydrothermal method is one of the popular method used because it is simple, inexpensive, involves low temperature, produces high yield, is scalable and the process is more controllable. This method was used by Kiomarsipourn et al. [34] by preparing various pigments of ZnO on a large scale at low temperature without using supplements such as surfactants and templates. SPT is used to prepare transparent conducting oxides. This technique is very easy, has low cost, safe and good for the production of large area uniform film coatings [39]. The chemical bath deposition (CBD) technique is simple to perform at low temperatures, environmentally friendly, catalyst free and inexpensive [40].

Properties such as: the phase structure, the structural orientation and amorphous state of the material are obtained from analysing the XRD pattern. Gandhi et al. [41] and Norton et al. [42] show in their studies that ZnO shift from diamagnetic behaviour to ferromagnetic behaviour when ZnO nanoparticles is doped with cobalt (Co) and this has also being predicted theoretically [43]. Karak et al. [44] reported that the XRD pattern of the undoped and cobalt doped ZnO appear as single phase of hexagonal wurtzite structure, which indicate the Co ions was successfully doped throughout the ZnO lattice [45]. Even though from the same pattern of XRD there is a shifting of diffraction peaks to the higher angle for those doped ZnO pattern and this might be the fact that the ionic radius of cobalt (0.58 Å) is smaller compared to the ionic radius of zinc (0.60 Å) [46]. Also Cong et al. [47] and El-Hilo et al. [48] reported on Mn doped ZnO, where no disturbance occurred when Mn were introduced in the structure. On the studies of Lamba et al. [49], a clear EDS spectra of ZnO doped SnO_2 nanoparticles

prepared by facile hydrothermal process shows only serveral peaks of Zn ,Sn and O are well difined, which reveals that the prepared material does not contain impurities.

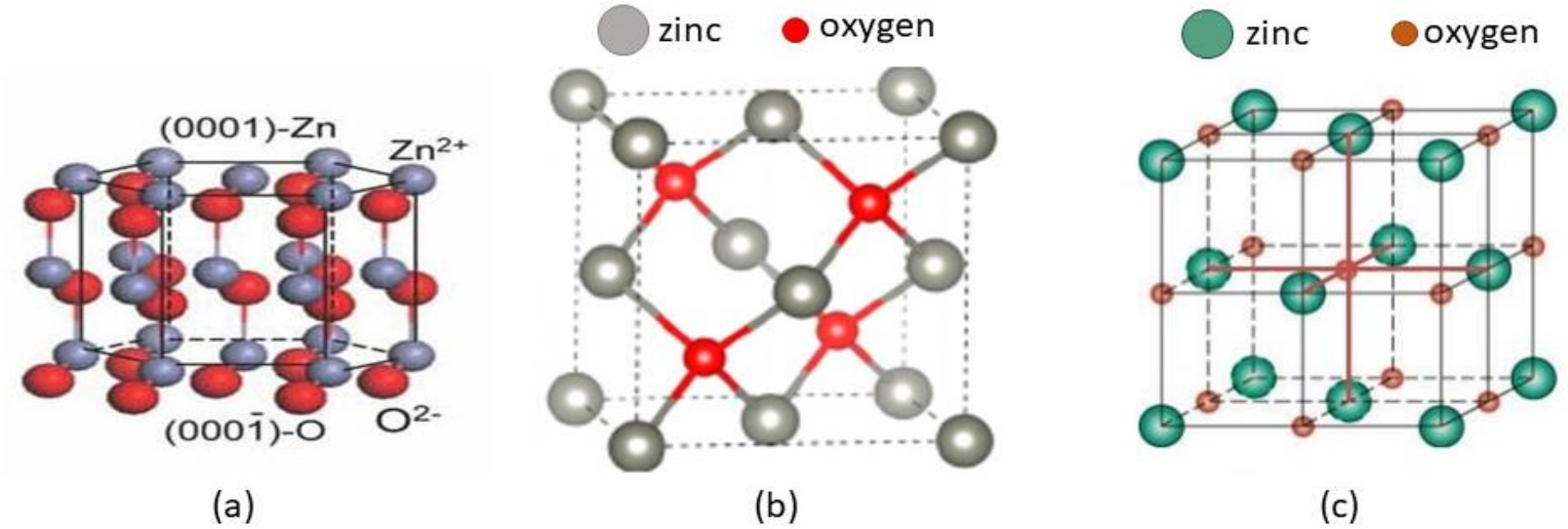

Figure 2. 1 (a) Hexagonal (Wurtzite) [50], (b) Zincblende (ZB) and (c) Rocksalt (RS) model of ZnO nanostructures.

The ZnO nanostructures can be obtained either in gaseous phase or in a solution form. The gaseous phase is the least explored method as compared to the solution phase because it's complicated and expensive [51]. The hexagonal WZ ZnO is observed under normal pressures [52]. It is transparent in the visible light range and it has been reported that dopants such as (B, Al, In, Ga) of group III and (Pb, Sn) in group IV can enhance its conductivity [53]. At Zn-rich conditions ZnO is considered as n-type semiconductor [54]. Studies show that n-type doping of ZnO is more adaptable as compared to the p-type doping [55]. The polar surface is an important characteristic of ZnO, in which basal plane (0001) is the common polar surface [56]. Zn^{2+} and O^{2-} are the two interconnecting sub-lattices found in the ZnO crystal structure [57], along the c-axis each Zn^{2+} ions is surrounded by a tetrahedral of O^{2-} ions and vice-versa [58], meaning the one end is partially positive zinc lattice site; Zn-(0001) and the other partially negative oxygen lattice site; O-$(000\bar{1})$, see figure 2.1 (a). ZnO has two most observed facets namely $\{2\bar{1}\bar{1}0\}$ and $\{01\bar{1}0\}$ which are non-polar and have lower energy than the {0001} facets [56].

Semiconductors such as ZnO, CdS and ZnS can be cubic zincblende (ZB) and hexagonal wurtzite (WZ) [59]. The ZnO RS and ZB crystal structure have their conventional unit cell as cubic while the WZ crystal structure has a hexagonal lattice [60]. This cubic phase has been reported as metastable at atmospheric pressures [61]. The lattice parameter for rocksalt is a= 4.283 Å [62] and for zinc blende is a= 4.62 Å [63]. The ZnO nanoparticles transform to Rocksalt (RS) nanoparticles structure at high pressures. These transformations were studied both theoretically [64], [65] and experimentally [66, 67]. The stability of the RS phase can be increased by doping ZnO with Mg, Mn, and Co metals [68]. While the First-principle calculations done by Zhang et al. [68] and Wang et al. [69] shows that the transition pressure from WZ-RS

decreases when Mn and Co dopants are introduced. The index direction of ZB-ZnO is [011], [70].

2.2 Optical properties of ZnO

Defects are unavoidable and they are contained in every material, hence there is no such thing as perfect materials. Crystal defects can be of single atom, row of atoms and ensemble atoms which explains the existence of point defects, line defects and complexes. There are two distinct deep level defect(s) of emission; namely intrinsic and extrinsic level defects. Vacancies such as zinc vacancy (V_{Zn}) and oxygen vacancy (V_O) are classified as the intrinsic level defects, while the interstitials and substitutional such as zinc interstitial (Zn_i), oxygen interstitial (O_i), zinc anti-site (Zn_O) and oxygen anti-site (O_{Zn}) are classified as the extrinsic level defects [71]. These type of defects are found in ZnO nanostructures and prediction shows that ZnO is a semiconductor that contained a large number of point defects that influences its thermal conductivity [72]. The intrinsic defects control the electrical conductivity of ZnO since they act as n-type donors. The electrical resistivity property decreases when ZnO is doped with group III elements [73, 74]**.**

ZnO is classified as a compound semiconductor. Its band gap can be controlled by adjusting the carrier concentration with donor such as the oxygen vacancies (V_O) and interstitial zinc (Zn_i) atoms [74]. The performance of these semiconductors can be improved by introducing dopants into the lattice of the SMOs [75]. Wang et al. [76] reported about ZnO nanocrystal doped with Mg were the absorption spectrum shows a blue shift indicative of an increase in the band gap, but Cd-ZnO nanocrystal indicate a decrease in band gap as the doping concentration of Cd increases from 0-10 %.

Wang et al. [77] reported about ZnO nanoparticles synthesised by colloidal chemistry method in which state that as the crystallite size increases the oxygen vacancy decreases, leading to the increase in UV emission. When ZnO nanoparticles are doped with Cu^{2+} ions they do not change the crystal structure, instead they increase the energy band gap up to 3.93 eV [78]. Even Tong et al. [79] report shows the band gap of ZnO nanoparticles increases as the doping concentration of Mn^{2+} increases. This is due to the substitution of Zn^{2+} ions in the ZnO lattice by Mn^{2+} ions. The thickness of the film has a great influence on the structural, optical and electrical properties of ZnO thin films. When the grain size increases, the thickness of the film also increase, thus the crystalline quality of the films gets better. Prasada et al. [80] also reports that the heat treatment improves the electrical conductivity of ZnO thin films. But while doing that we should also keep in mind that the charge carrier concentration increase at higher temperatures while the Debye length decrease. This indicates that a temperature has an effect on the semiconducting sensor material and this changes the physical property of a material as reported by Mizsei [81].

The optical properties are influenced by the energy band structure and lattice dynamics [82]. ZnO nanostructure has a band gap of 3.4 eV which is suitable for short wavelength optoelectronic applications [83]. SnO_2 and In_2O_3 are weak n-type semiconductors with band gap of 3.62 eV [84] and 2.9 eV [85], respectively. They both exhibits great electrical and optical properties [86, 87]. Like SnO_2 which possess low electrical resistance and high transparency in the UV-visible region [88]. SnO_2 has a rutile crystal structure while In_2O_3 has a cubic crystal structure [89]. Even CdO is a face centred cubic (FCC) crystal structure with very low band gap of 2.28 eV. CdO is less desirable because of the cadmium (Cd) for its toxicity [90].

2.3 Sensing properties of ZnO

The most important parameters in developing gas sensors are sensitivity and selectivity which draw attention of many researchers. Sensitivity can be defined as R_g/R_a for oxidizing gases and R_a/R_g for reducing gases, where R_g is for the resistance in the reference gas containing target gases and R_a is for the resistance of gas sensors in the reference gas (usually the air). There is a significate relationship between R_g and R_a with the surface reaction(s) taking place [91].

$$\text{sensitivity}(S) = \frac{R_a - R_g}{R_a} = \frac{\Delta R}{R_a} . \qquad (2.3.1)$$

The transition metal oxides (TMO) are solid materials normaly tested for gas sensing applications; for example we have WO_3, SnO_2, ZnO, and In_2O_3 which are the most investigated group of sensors among other types reported recently by Gurlo [92]. Figure 2.2 shows the schematic diagram of static gas system that is similar to the one which Gurlo [92] used to test all those gases. These TMO have large band gap ranging between (3 eV - 4 eV) [93] and are expected to be quite inert under normal temperatures. They have an excellent electrical and optical characteristics and are known to be transparent within the visible electromagnetic region of about 400 nm to 700 nm [94]. They are amorphous materials and also known to be very conductive in their amorphous state [95]. Among the semiconducting material, In_2O_3 has been studied for possible chemical sensing due to its advantageous features such as a wide band gap of about 3 eV, good catalysis and low resisistivity [96]. But in the ZnO structure, the crystal defects such as the oxygen vacancies or shallow donor are the key factors in determining the gas sensing properties, since they play a role in the absorption sites for the gas molecules and along the ZnO nanostructure surface [97]. Sensors are extremely important in detecting toxic and flammable gases such as CH_4,

H_2, NH_3, H_2S and CO in mines, gas storage plants, petroleum industries and households [98]. This helps in maintaining healthy working and living environment, to avoid risk of accidental explosion and public safety in general. H_2 is the most useful gas in many chemical processes and numerous industries including aerospace, petrochemical, medical and energy [99]. This gas has a perfectly clean combustion action which does not release any pollutants or greenhouse gases, thus making it a promising clean energy source for future generation of autmobiles and household appliances. However, when H_2 is concentrated in air by about 4% to 75% by volume, it may cause explosions. Bearing in mind that H_2 is a colourless, odorless and testeless gas that human sensors can not detect [99, 100]. On the other hand there is CO which is colourless and odourless. This gas has the highest contribution to air pollution. CO is usually produced by incomplete combustion of industrial and domestic fuels jointly with veld fires [101]. There is also H_2S gas which is also colourless, flammable with a very bad smell produced from city sewage, hot springs, natural gases, gasoline and volcanic gases. H_2S smells rotten eggs and is a highly toxic chemical gas which can lead to unconsciousness or death even at low concentrations [102, 103, 104, 105]. Semiconductor sensors such as WO_3, ZnO, In_2O_3 and some perovskite type materials have been found to be sensitive to H_2S gas. ZnO were reported to show high sensitivity with fast response and recovery time for low concentration of H_2S gas [106]. Wang [107] reported that the morphology of the nanoparticles have high sensitivity and quick response to the gases because they are 1-dimensional. It has being verified both experimentally and theoretically for various sensing materials like In_2O_3 and SnO_2 that the decrease in crystallite size exhibit an increase in the sensor response. Parthbavarman [108] reported that doping with Co can enhance the sensing behaviour of TMO, and also the detection of ethanol gas were performed using Co-doped SnO_2

nanoparticles. There are many materials which are being used for sensing applications but they are not effective and often suffer from low sensitivity, slow response, poor selectivity and slow recovery time.

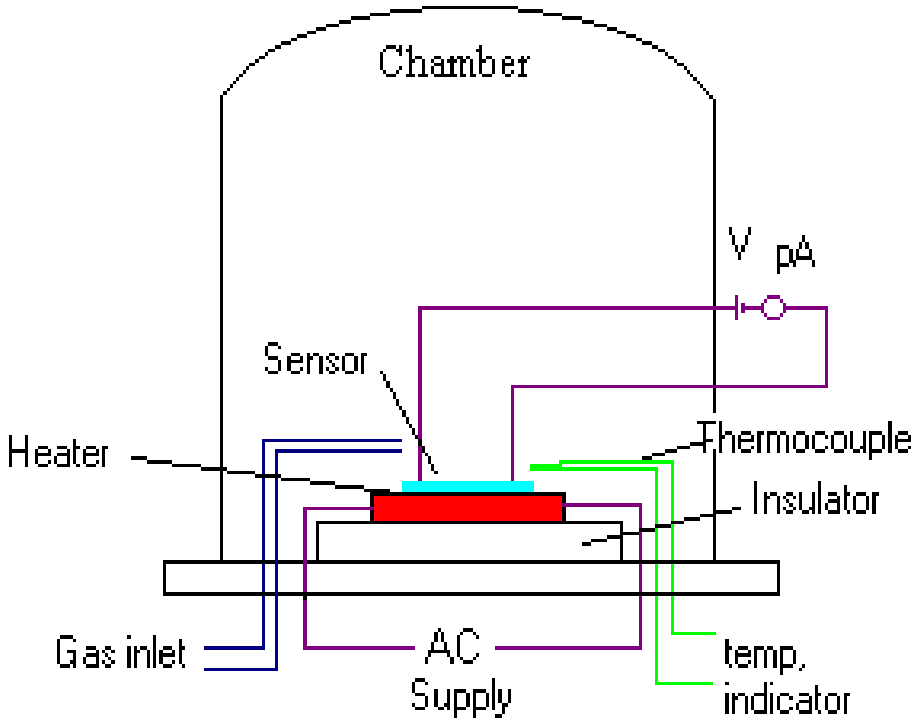

Figure 2. 2: Schematic diagram of static gas system according to Gurlo *[92]*.

Chapter 3

Experimental techniques and characterisation

3.1 Methodology

Zinc oxide (99.9 %), cobalt (99.8 %) and indium (99.9 %) where purchased from Sigma-Aldrich and used without further purification. The undoped ZnO, Co-ZnO and In-ZnO nanoparticles were synthesised mechano-chemically using an 8000 MIXER ball milling machine [109] for 12 hours doped by 2 %wt, 5 %wt and 10 %wt. This was attained by directly putting proportionate amounts of ZnO and Co or In into the steel vial. The double doping ZnO nanoparticles with two metals cobalt and indium were also performed as follows: 2 %wt (1% In/ 1% Co), 5 %wt (2.5% Co/ 2.5% In) and 10 %wt (5% Co/ 5% In) doped and ball milled for 12 hours as well. 3 g of ZnO powder was measured and placed into the hardened steel vial (that can grind up to 10 g of the sample) with two stainless steel balls of diameter 6.825 mm.

3.2 Ball milling

Ball milling machine also called a shaker mill, the SpexMill or high-energy ball mill has been utilised for mechano-chemical synthesis. It comes with 8001 hardened steel vial set and a set of different sizes of stainless steel balls having different diameters. It has safety interlock system, a variable-range electronic timer, and shock-mounted electric motor for table top operation. It runs for 0-100 minutes and it can be extended to 1000 minutes or more by the user. It can grind up to 10 g of a sample and up to 60 mL for blending powders. An extensive part of the machine’s limitations lays in the fact that the particles are characterized only by size [110].

(a)

(b)

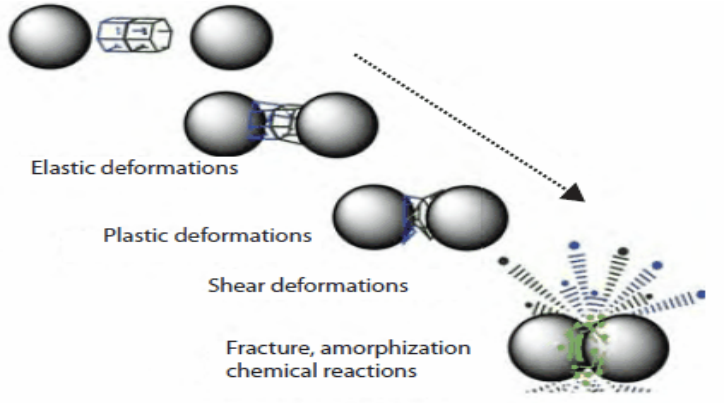

(c)

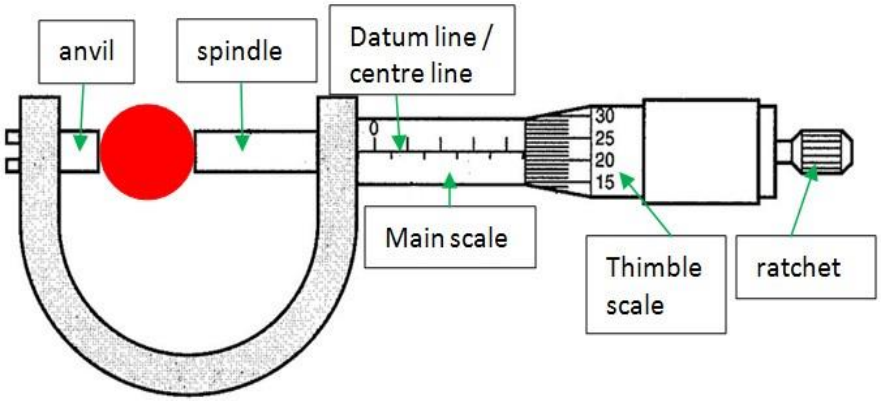

(d)

Figure 3. 1: (a) 8000M Mixer/Mill, (b) 8001 hardened steel vial set, (c) Changes in the material trapped between colliding balls in a ball mill and (d) micrometer screw gauge.

This ball milling machine has served analytical chemists and spectroscopists for over forty years. It has being used for grinding or mixing raw materials for further processing. Each ball develops fairly high G-forces, enough to grind the samples into powder-like substances (analytical fineness) as the machine shake the vial in complex motion of back-and-forth swing. It can also be utilized for mechanical alloying and nano-milling [111]. A 8000M Mixer together with its contents are shown in figure 3.1.

3.3 Characterisation techniques

Characterisation of the samples was carried out using X-ray diffraction (XRD), Scanning Electron Microscopy (SEM), Raman Spectroscopy (RS), Photoluminescence (PL), Ultraviolet-visible (UV-vis) spectroscopy and the kenosistec station equipment.

3.3.1 X-ray diffraction (XRD)

The XRD experiment were performed using the Phillips analytical X-Ray B.V diffractometer machine with Cu $K\alpha_1$ (λ= 1.54 Å) monochromatic radiation source. The measurements were collected at 45.0 keV and 40.0 mA. The XRD were collected by scanning between $2\theta = 20^o$ and 60^o in 0.02^o steps. Figure 3.2 shows the schematic diagram of a usual X-Ray powder diffractometer. The average crystal size was determined using the Debye-Scherrer's formula [112]:

$$D = \frac{k\lambda}{\beta_{hkl} cos\theta}, \qquad (3.3.1.1)$$

where *k* is a constant of 0.9 (the shape factor for spherical surface), the wavelength (λ) of X-rays (λ=1.54 Å for Cu $K\alpha_1$ radiation), β is the full width at half maximum (FWHM) and theta (θ) of the Bragg's angle.

The strain induced in powders due to crystal imperfection and distortion were related by:

$\varepsilon = \frac{\beta_{hkl}}{4tan\theta}$. (3.3.1.2)

Now, a different approach is employed where the total integral breadth of Bragg peak is obtained by adding the crystallite size and the strain broadening components [113].

From equation (3.3.1.1) and (3.3.1.2) it is clear that the peak width from crystallite size varies as $\frac{1}{cos\theta}$, whereas the strain varies as $\tan^{-1}\theta$. Combining the Scherrer's equation and $\varepsilon = \frac{\beta_{hkl}}{4tan\theta}$ results in the Williamson-Hall equation [114]:

$\beta_{hkl} = \beta_D + \beta_s$, (3.3.1.3)

$\beta_{hkl} = \frac{k\lambda}{Dcos\theta} + 4\varepsilon\tan\theta$. (3.3.1.4)

Rearranging equation (3.3.1.4) gives:

$\beta_{hkl}cos\theta = \frac{k\lambda}{D} + 4\varepsilon\sin\theta$. (3.3.1.5)

The d-spacing was calculated using the Bragg's law:

$2d_{hkl}sin\theta = n\,\lambda$, (3.3.1.6)

where $d_{hkl}$is the interplanar spacing, n is an integer specifying the order of diffraction and θ is the diffraction angle.

The following equation relate the interplanar spacing to the (h k l) planes and lattice constants a = b and c in the hexagonal structure of ZnO.

$\frac{1}{d_{hkl}^2} = \frac{4}{3}\left(\frac{h^2+hk+k^2}{a^2}\right) + \frac{l^2}{c^2}$. (3.3.1.7)

Where a = b ≠ c are lattice parameters. Now for plane orientation (100), the lattice constant is calculated using the following relation:

$$a = \sqrt{\frac{4}{3}(d_{hkl})^2}. \quad (3.3.1.8)$$

Now for the plane orientation (002)

$$c = \sqrt{4(d_{hkl})^2}. \quad (3.3.1.9)$$

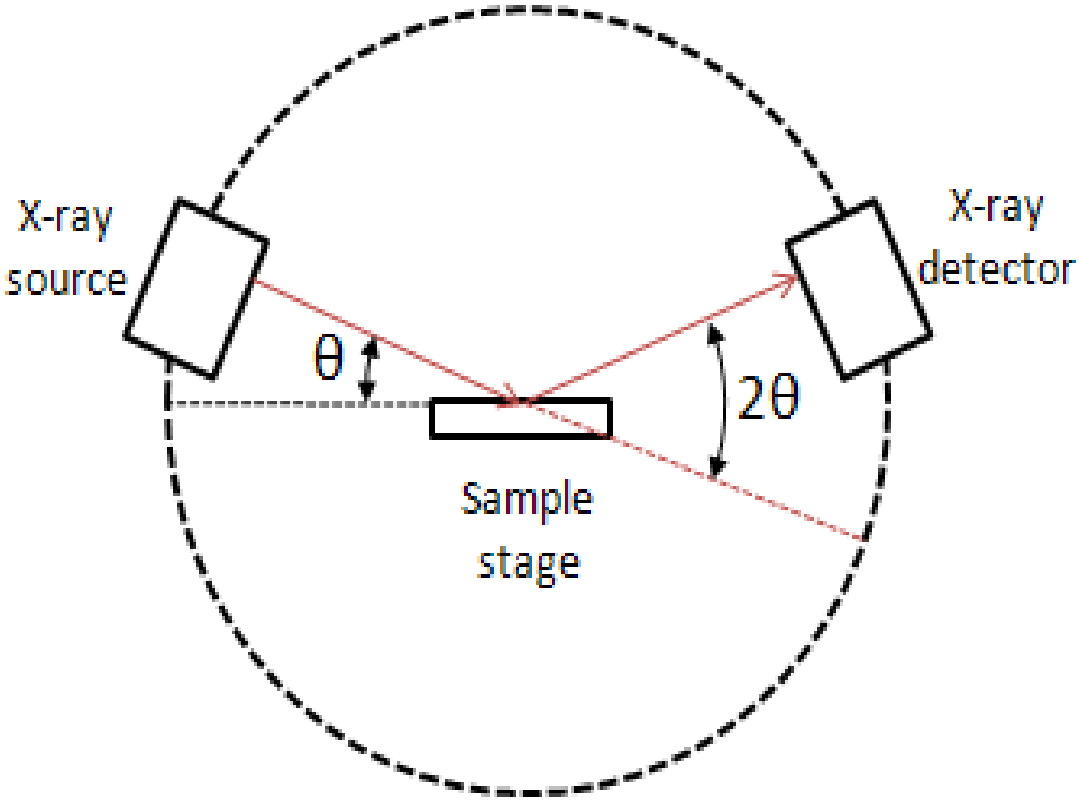

Figure 3. 2: The schematic diagram of X-ray powder diffractometer (XRD) *[115]*.

3.3.2 Scanning Electron Microscope (SEM)

When preparing the samples for SEM characterization, acetone is used to clean the aluminium-stub. Thereafter a carbon tape is placed on the stub so that the ZnO nanoparticles can be deposited on it. When taking the SEM images, an electron beam is emitted from the electron gun, see figure 3.3. The anode determines the accelerating voltage of the gun and also polarises the electron beam. The magnetic lens magnify the image of the beam source exciting the electron gun and to focus the beam on the specimen [116]. There are also scanning coils which operate to control the raster of the beam and to construct the image from point to point [117]. Those electron beams will interact with the sample and create the secondary electrons which are collected in the secondary electron detector (SED) to create an image [118]**.** A mechanism of how a SEM creates images is shown in figure 3.3.

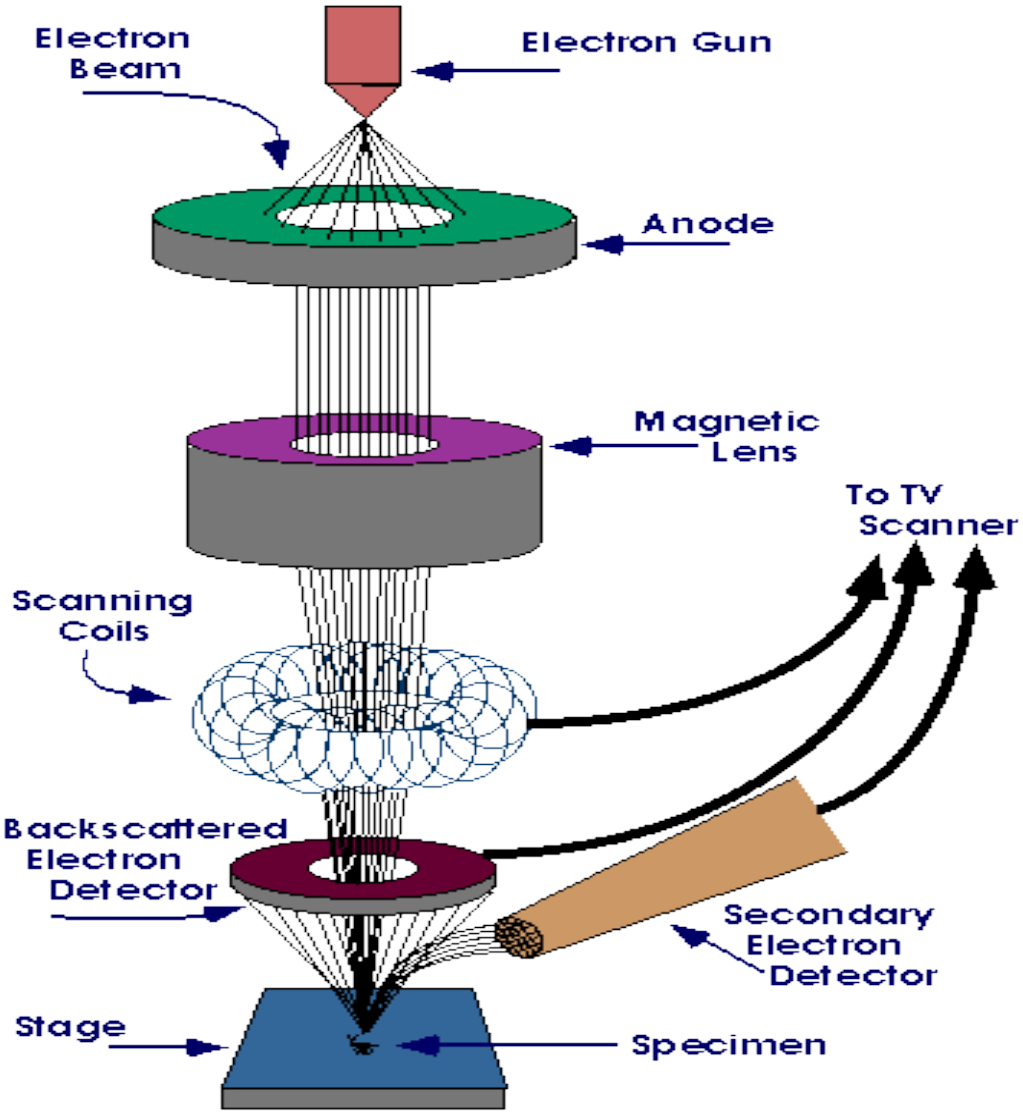

Figure 3. 3: Scanning electron microscope (SEM) *[119]*.

3.3.3 Photoluminescence (PL) spectroscopy

PL spectroscopy is a contactless, non-destructive method of probing the electronic structure of materials. It also provides more information on bandgaps, defect identification and material quality. Light is directed onto a sample, where it is absorbed and imparts excess energy into the material in a process called photo-excitation [120]. PL originates from absorption or emission process experienced in different energy states in a sample [121]. A PL spectroscopy instrument is pictured in the figure 3.4 below.

Figure 3. 4: $Nano_{Log}$Photoluminescence.

3.3.4 Ultraviolet-visible (UV-vis) spectroscopy

The UV-vis spectrometry is used to measure the transmittance, reflectance and absorption of the sample. A UV-vis spectrum can be otained when the electromagnetic radiation of diverse wavelength (near UV and near IR) is ideally irradiated on to the sample. Hence, a monochromatic radiation is employed at a time. The spectrum is a measure of the radiation absorbed at each wavelength against the wavelength [122]. The position of the maximum of the absorption band called λ-max, and the intensity of the bands are the two major parameters used to characterise the UV spectra of substances [123]. Even the energy band gap of the materials is calculated from the UV-vis data [124]. A schematic diagram demonstrating how a UV-vis spectrophotometer generates data is shown in figure 3.5.

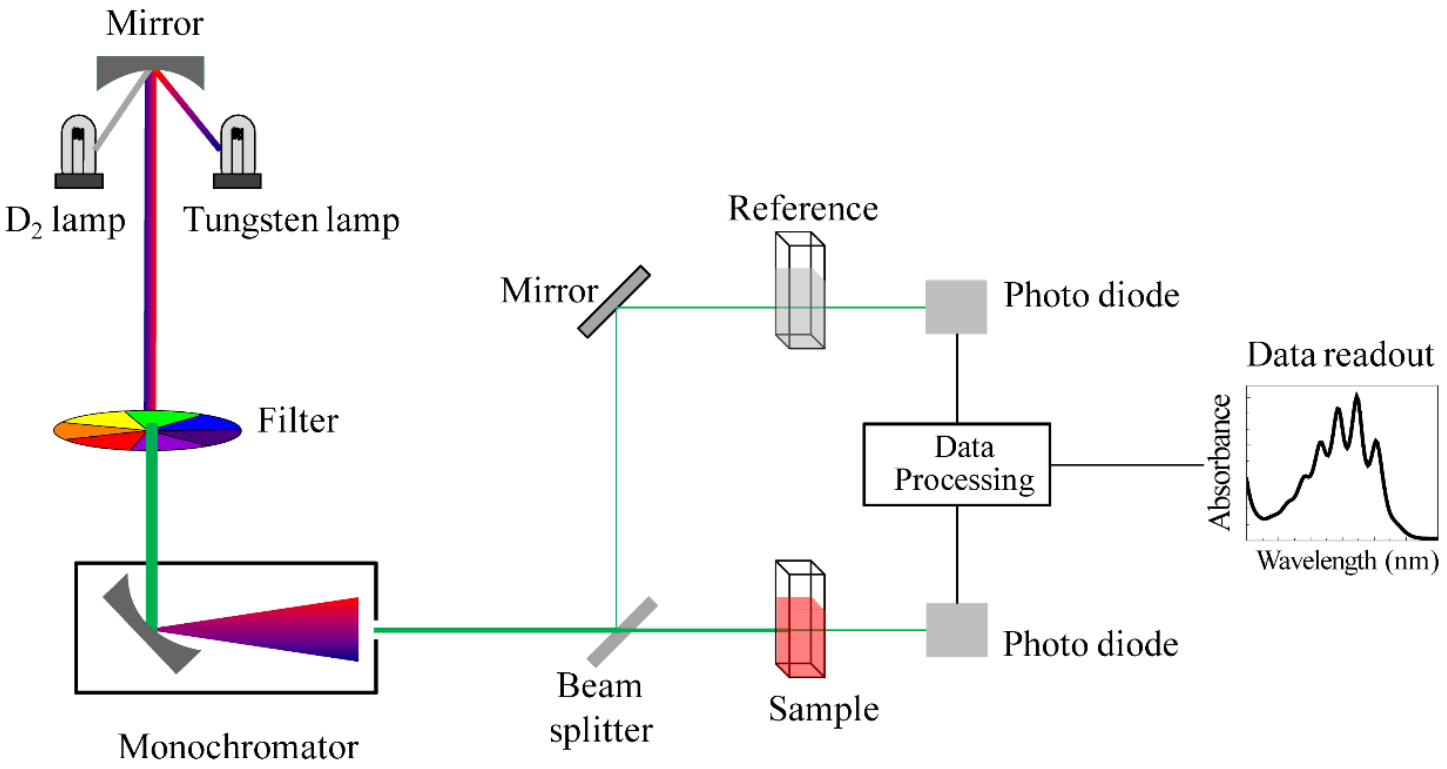

Figure 3. 5: The schematic diagram of UV-visible spectrophotometer (UV-vis) *[125]*.

3.3.5 Raman spectroscopy (RS)

RS is used to determine modes of molecular motions, especially vibrations [126], [127]. The RS is obtained by illuminating a monochromatic laser beam on to a sample to generate a scattering light. Now only the wavelength different to that of the incident light is analysed. It is applicable to the qualitative and quantitative analysis of covalently bonded molecules [128]. The instrument is used for identification of phases, molecular and crystalline symmetries, crystalline polymorphs and measurement of stress. RS databases are used to plot a spectrum (a graph of light intensity as a function of light frequency) of the measured results [126]. The peaks in the spectrum provide information about molecular structure and from the molecular structure, the compound constituents can be identified [129]. A raman spectroscopy equipment picture is shown below in figure 3.6.

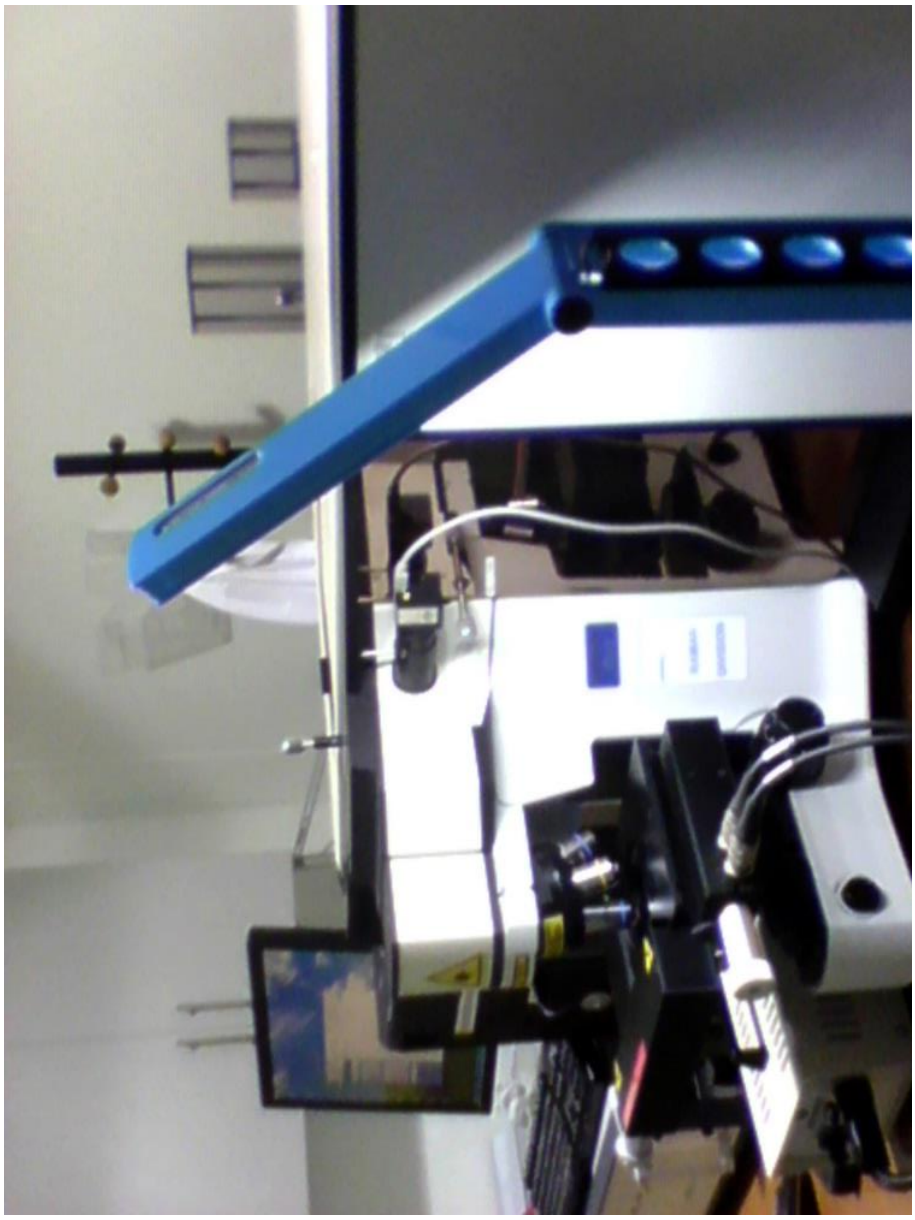

Figure 3. 6: Raman spectroscopy (RS).

3.3.6 The kenosistec station equipment

The kenosistec station equipment is used to test the prepared compound materials such as SnO_2, ZnO etc. for gas sensing response, operating temperature, recovery time and more. A sample is placed on the micro-hotplate sensor [130] and thereafter all the grouping is placed in the machine where there are two channels; one responsible for the flow of current and the other for the flow of heat. When the sample is in the machine, one type of gas pipe is open for some time for a particular concentration to infiltrate the sample area. The gas pipe is then closed in order to observe the recovery and response time of the material. This is done for constant time while varying gas concentration and temperature for different gases such as the carbon monoxide (CO), methane (CH_4), hydrogen (H_2), ammonia (NH_3) and sulphurous gases (H_2S, SO_2) [131]. In order to analyse what material detects which gases best, graphs of response (R_a/R_g) against time (s), temperature (^oC) and concentration (ppm) are plotted from the measured data. Now the type of material produced limits the sensing ability in a sense that if Cu-ZnO nanoparticles detect only NH_3, even if CH_4 is present in the area it would not be able to detect it [132, 133, 134]. The kenosistec station equipment is shown in the figure 3.7 below.

Figure 3. 7: The kenosistec station equipment.

Chapter 4

Structural and optical properties

4.1 Introduction

Zinc oxide (ZnO) is a promising inorganic n-type semiconducting metal oxide. Its physical and optical properties are important for short-wavelength optoelectronic applications with a wide band gap of about ~3.3 eV [135]. This material enjoys superfluous advantage such as low cost, rich material source, non-toxicity and low temperature synthesis, as compared with other semiconductors like GaN and CuO [136, 137]. The investigations reveal that the crystal structure of a material hold routes to various applications [138]. ZnO has being found to have a large family of nanostructures including nanowires, nanorods, nanoballs, nanosheets and so on. The nano- scaled properties enhances the applications of manufactured macro- devices such as smart windows, gas sensors, solar cells, and ultraviolet light-emitters [139]. Djerdj et al. [140] investigated the ferromagnetic behaviour of ZnO nanoparticles, and obtained that they possess more strength when doped with Co metal. Literature reports by Donesha and Jayanna et al. [141] indicate that the crystal structure of ZnO does not change when co-doped by Fe and Co. Many methods are being developed in order to produce nanoparticles of controlled size, such as ZnO nanoparticles [142]. As such, sol-gel method, one of the well-known technique was used by Spanhel et al. [143], Bahnemann et al. [144] and Maswanganye et al. [145] to prepare zinc oxide nanoparticles. The aim of this work is to study the structural and optical properties of ZnO nanoparticles prepared using high energy ball milling method, as it has been found to be adaptable and can be followed easily.

4.2 Structural characterisation

4.2.1 X-ray diffractometer (XRD)

The crystal structure of ZnO nanoparticles was investigated using XRD having incident Cu $K\alpha_1$ radiation (λ = 1.541 Å). The XRD results were collected by scanning the samples with diffraction angle between 2θ=20 and 60^o in 0.02^o steps. In figure 4.2.1 there is an XRD pattern which exhibit several diffraction peaks that can be indexed as hexagonal wurtzite structure, since peaks at 2θ = 31.77, 34.43, 36.27, 47.56 and 56.63˚ belonging to the (100), (002), (101), (102) and (110) planes respectively (JCPDS No.36-1451) were observed. This implies that the Co^{2+} ions were successfully incorporated into the lattice position of Zn^{2+} ions. Looking at the XRD pattern of In-ZnO nanoparticles, a new peak along the (400) plane (*) was observed between 31.78^o and 34.44^o. This peak is associated with an indium dopant [146]**.** Speculation were that Co^{2+} prefers the interstitial site which leads to great stress in the structures when compared to filling in a Zn^{2+} vacancy of which In^{3+} seems to be preferring. The crystallite size, strain and lattice parameters of undoped ZnO, Co doped ZnO, In doped ZnO and Co-In doped ZnO nanoparticles are listed in table 4.1. The results show the crystallite size of Co-ZnO nanoparticles being the largest of all the calculated nanoparticles, except for the purchased ZnO sample. When looking at the strains, the reverse was observed. The explanation could be extracted from the ionic radii of both In^{3+} and Co^{2+}. Since the ionic radius of Zn^{2+} is 0.60 Å while that of In^{3+} is 0.62 Å which is greater than that of Co^{2+} 0.58 Å [147]. The fact that strain values are consistently higher for Co-ZnO nanoparticles than for In-doped ZnO nanoparticles may point to the varying preferred sites of Co^{2+} and In^{3+} in the ZnO structure. It can also be observed that the crystallite size of all the single doped ZnO nanoparticles are larger than those of the double doped ZnO nanoparticles. Another fact is the crystallite sizes calculated

using Debye-Scherrer's equation [148] are large compared to the ones calculated by Williamson-Hall equation [149]. This is caused by the contribution of the strain parameter calculation that is included in the Williamson-Hall equation and not in the Debye-Scherrer's equation. While the strain of single doped ZnO nanoparticles are smaller than those of double doped ZnO nanoparticles. The percentage difference between the reported lattice parameters [150, 22] and the calculated ones are comparable.

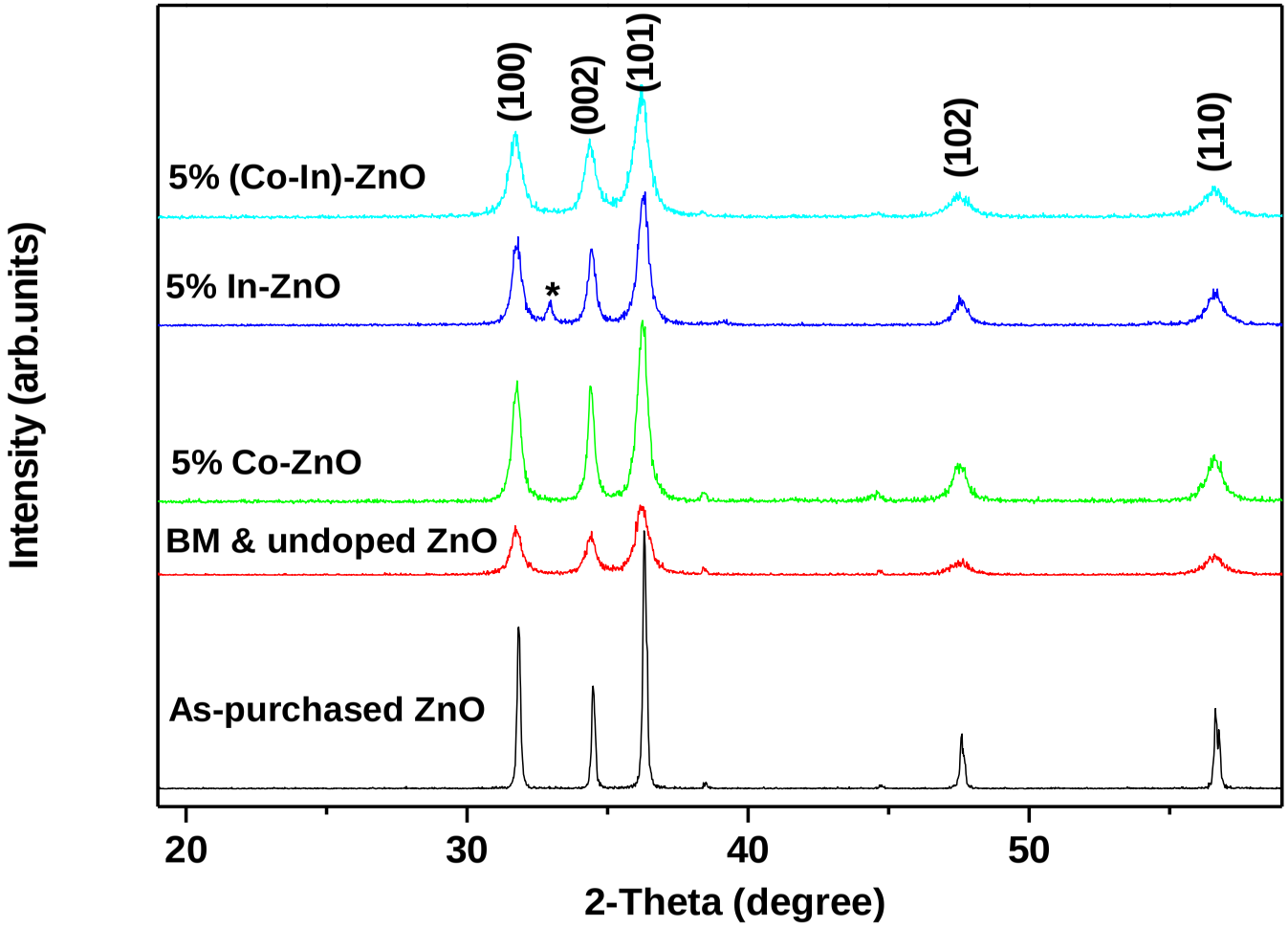

Figure 4.2.1: XRD pattern of the undoped and 5 %wt doped Co-ZnO, In-ZnO and (Co-In)-ZnO nanoparticles milled for 12hours.

Table 4. 1: The calculated crystallite size (by Williamson-Hall and Debye-Sherrer), strain and lattice parameters of 5% doped and undoped ZnO.

Sample name	Debye-Sherrer (nm)	Williamson-Hall (D) (nm)	Strain (ε)	Parameters (Å)	
				a=b	c
As-purchased ZnO	49.414	43.036	0.0015	3.252	5.210
Undoped ZnO	18.258	16.080	0.0057	3.251	5.208
Co-ZnO	21.791	18.804	0.0047	3.250	5.207
In-ZnO	20.570	17.765	0.0048	3.249	5.204
(Co-In) ZnO	15.354	13.263	0.0064	3.254	5.211

4.2.2 Scanning electron microscope (SEM)

The Joel [JSM-75OOF] model of SEM was used to examine the morphology of the ZnO nanoparticles. The images were taken at 100 nm scale and a magnification of x50. The SEM images appear to be spherical in shape as shown in figure 4.2.2 (a) and (b) for undoped ZnO nanoparticles and co-doped ZnO nanoparticles. The morphology of the ZnO nanoparticles were not significantly affected by the dopants added.

The energy dispersive spectroscopy (EDS) shows all the elements present in the sample (Zn and O); see figure 4.2.3 (a) for undoped ZnO nanoparticles. The elemental composition of the undoped ZnO nanoparticles was analysed and found to have Zn = 46.57, O = 26.90, C = 25.02 and Al = 1.51. The samples were mounted on carbon (C) tape, hence the presence of the weak C peak on the EDS spectra. The EDS of the undoped ZnO nanoparticles show the presence of a peak that belongs to aluminium element. This was caused by the aluminium step used when collecting data from the

SEM. There are several peaks for Zn in the EDS spectra as compared to other as ZnO was the host material.

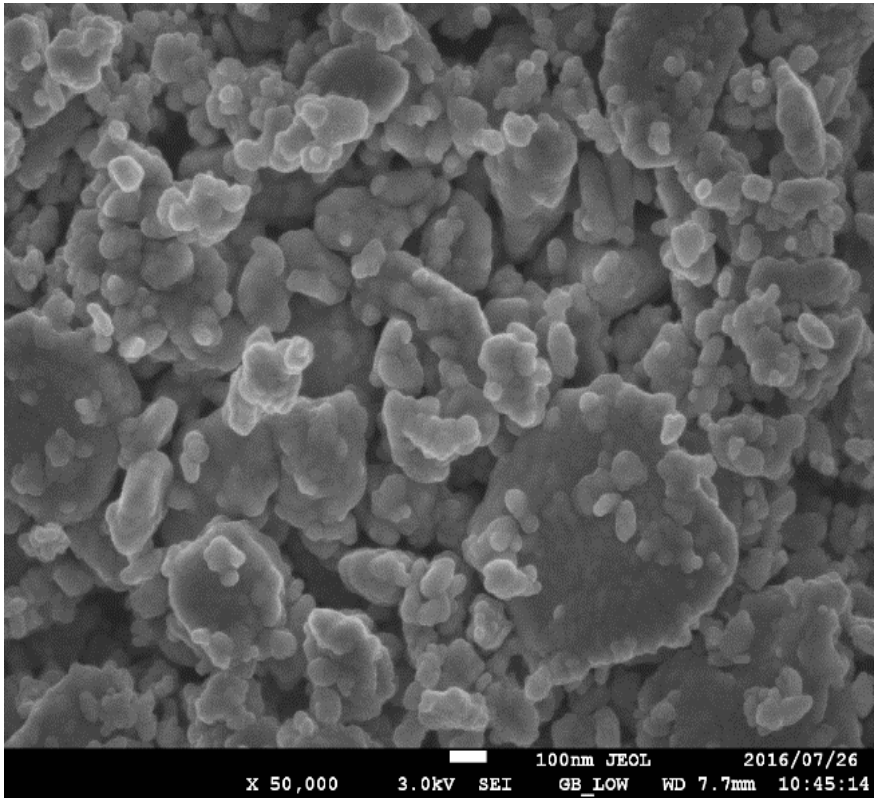

(a)

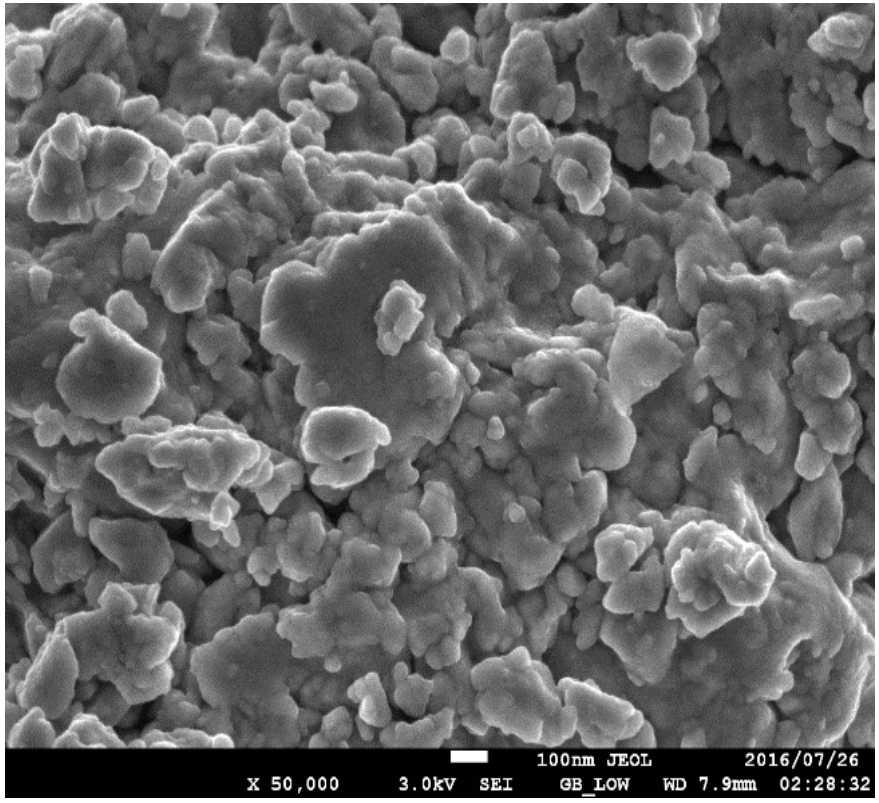

(b)

Figure 4.2.2: (a) The SEM of undoped ZnO nanoparticles (b) The SEM of 5 %wt co-doped (Co-In)-ZnO nanoparticles.

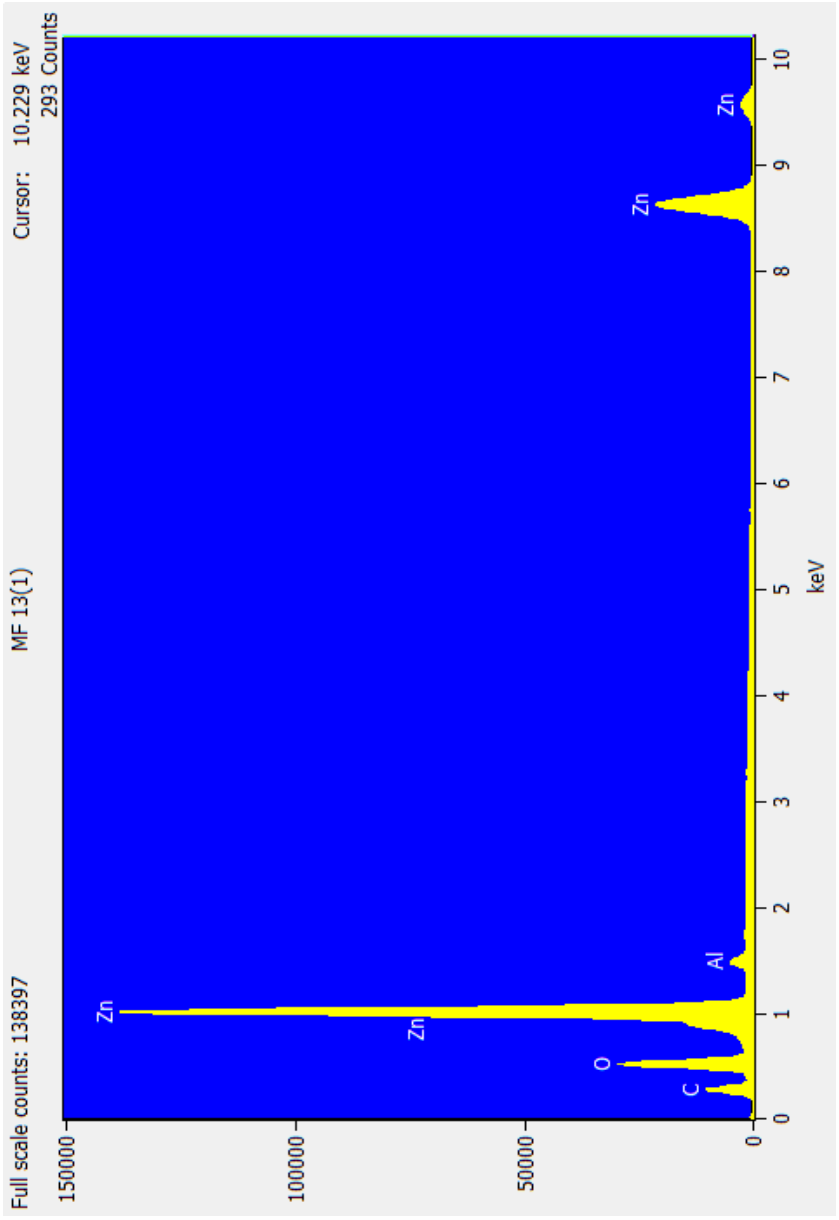

Figure 4.2.3: The EDS of undoped ZnO nanoparticles.

4.3 Optical characterisation

4.3.1 Raman spectroscopy (RS)

The Raman scattering method was employed to probe the phase purity and the vibrational modes of the ZnO nanoparticles [151]. Figure 4.3.1 shows the room temperature Raman scattering spectra of the doped and undoped ZnO nanoparticles prepared mechano-chemically. It is well known that the hexagonal wurtzite ZnO display three vibration modes in the Raman spectra: A_1, E_1 and E_2. A_1 and E_1 modes split into two modes, namely longitudinal optical (LO) and transverse optical (TO) components respectively, while E_2 (high) mode also consists of two modes of low and high frequency phonons [152]**.** The intense peak observed at 436.4 cm^{-1} for the undoped ZnO nanoparticles is known as the Raman-active dominant E_2 (high) mode, indicating that all prepared samples are of the hexagonal wurtzite phase of ZnO [153]. The increase in the compressive stress on the sample cause the frequency shift to the blue region of E_2 (high) mode from 436.4 to 429.0 cm^{-1}. This is consistent with the XRD patterns as shown in figure 4.2.1. At a frequency of 329.6 cm^{-1} a peak associated with the E_{2H}-E_{2L} mode can be observed. The third peak centered at 573.5 cm^{-1} represent two modes: A_1 (LO) and E_1 (LO) modes that are superimposed. This peak is believed to result from intrinsic defects in ZnO nanoparticles such as oxygen vacancy, zinc interstitial, or their complexes [151, 154, 155]. The defects can also be observed in the PL spectra of the material which clearly confirms that the prepared samples are actually hexagonal wurtzite ZnO nanoparticles. It is observed in figure 4.3.1 that all the graphs of the doped ZnO nanoparticles experiences a blue-shift and they display the same pattern of mode. The intensity of the peaks decreases as dopants are introduced into the ZnO nanoparticles. The defects induce the internal

strain in the original nanoparticle structure [156]. In addition, the blue-shift is associated with the modification of the material property. The In-ZnO nanoparticles were observed to be favoured, hence the obtained frequencies are close to that of the undoped ZnO nanoparticles as compared to others. The position of the peaks obtained in figure 4.3.1, are in good agreement with what Schumm et al. [157] had obtained, where peaks at 329.5 cm^{-1}, 436.4 cm^{-1} and 573.5 cm^{-1} are for E_{2H}-E_{2L}, E_{2H} and A_1 & E_1 respectively for the excitation wavelength of 514.532 nm [158].

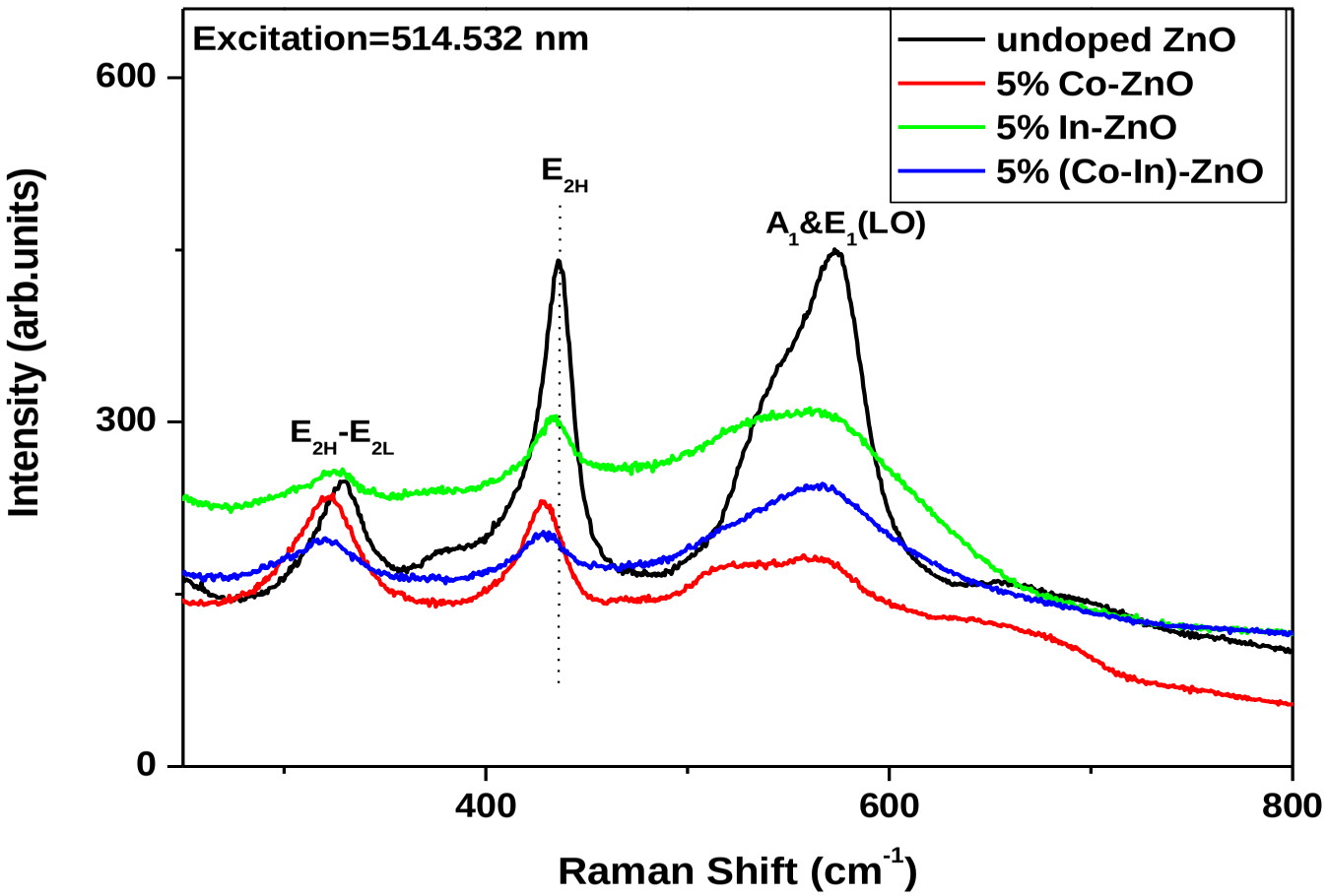

Figure 4.3. 1: Raman spectra of the undoped and 5% doped Co-ZnO, In-ZnO and (Co-In)-ZnO nanoparticles.

4.3.2 Ultraviolet-visible (UV-vis) spectroscopy

UV-vis absorption spectra were recorded using Perkin-Elmer Lambda 750S UV-vis spectrometer. This UV-vis spectrometer was used to probe the optical band gap of the doped and undoped ZnO nanoparticles along the wavelength range of 350-800 nm. The calculations were done using the following equation [22]**:**

$$E_g = \frac{hc}{\lambda}, \qquad (4.4.2.1)$$

here E_g is the energy band gap, h is the plank's constant (6.626×10^{-34} J·s), c is the speed of light (2.998×10^8 m/s) and λ cut off wavelength in nm. The cut off wavelength was determined by extrapolating a straight line along the absorption edges through the wavelength axis. A point where the straight line intercepts the wavelength axis is our cut off wavelength, see figure 4.3.2. The E_g for undoped and doped ZnO nanoparticles was also calculated and presented in table 4.2. The values obtained are ranging from 2.08 to 2.58 eV. The E_g of the co-doped (Co-In)-ZnO nanoparticles are much smaller than the Co-ZnO and In-ZnO nanoparticles. Previous literature by Wang et al. [159] shows that the bulk ZnO has the absorption edge at 387 nm in the UV-vis spectra which is obviously larger than that of the undoped ZnO nanoparticles (480 nm). Thus, the E_g of bulk ZnO is found to be greater than the E_g of undoped ZnO nanoparticles.

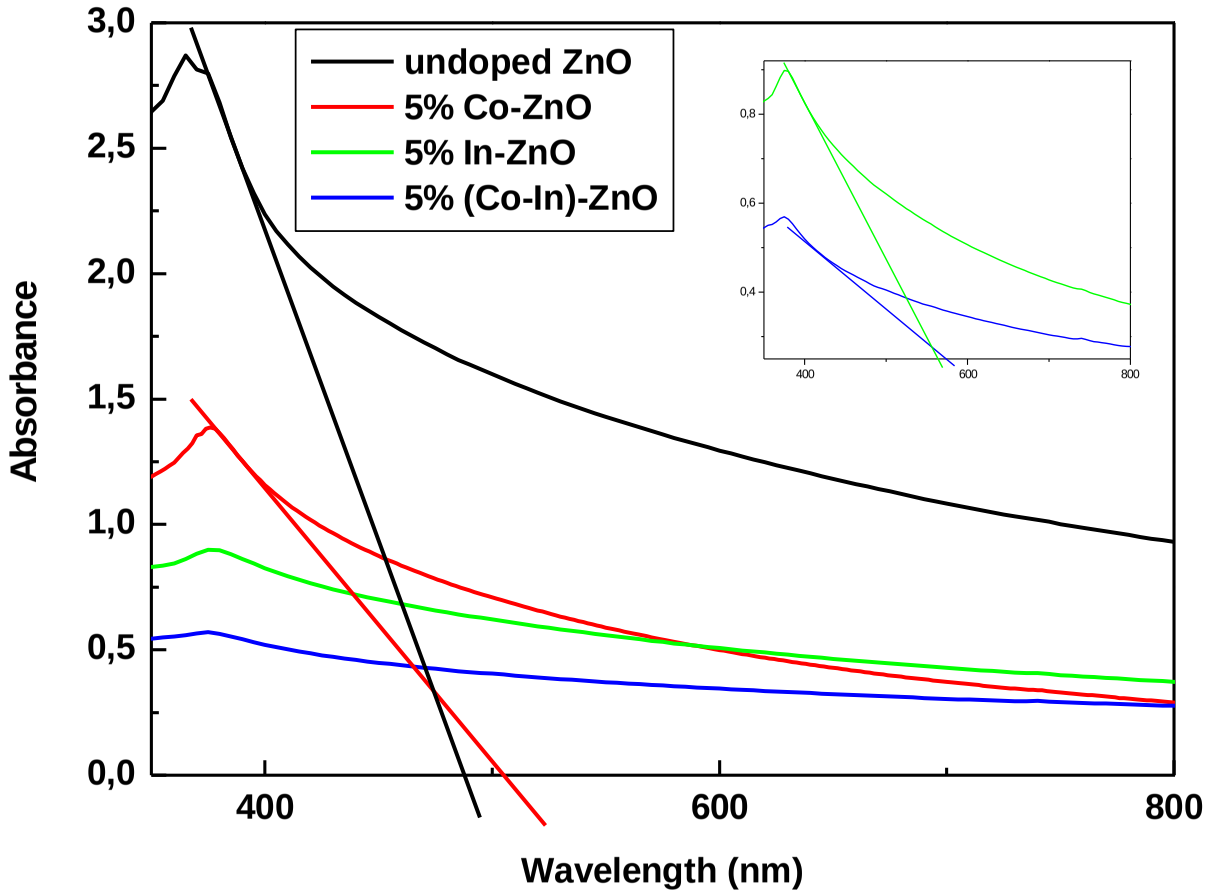

Figure 4.3.2: UV-vis absorption spectra for undoped and 5% doped ZnO nanoparticles.

Table 4. 2: The calculated energy band gap of the doped and undoped ZnO nanoparticles.

Sample	Doping (wt %)	Wavelength (nm)	Energy band gap (eV)
Bulk ZnO **[159]**	-	387.000	3.20
Undoped ZnO	0	479.917	2.58
Co-ZnO	5	509.830	2.43
In-ZnO	5	588.976	2.11
(Co-In)-ZnO	5	596.074	2.08

4.3.3 Photoluminescence (PL)

The NanoLog [*i*HR320 Horiba JOBINYVON] model of PL was used to collect data at room temperature. PL emission spectra of the undoped and doped In-ZnO, Co-ZnO and (In-Co)-ZnO nanoparticles are shown in figure 4.3.3. These spectra were obtained with an excitation wavelength of 350 nm. The first near band edge ultraviolet (UV) emission peaks that appear in the PL spectra are for In-ZnO and (Co-In)-ZnO centered on 380 nm, which is attributed to the excitonic recombination. This is the recombination of an electron in the conduction band and a hole in the valence band [160]. A higher blue PL intensity is due to the presence of high number of ionised oxygen vacancy defects [161]. In-ZnO and (Co-In)-ZnO samples display similar trend in the behaviour of intensity as a function of wavelength even though the intensities are differing. This outcome may indicate that the ZnO nanoparticles synthesised by the high energy ball milling technique may possess high crystalline perfection. The undoped ZnO nanoparticles shows three defects, namely zinc interstitial (Zn_i), zinc vacancy (V_{Zn}) and oxygen vacancy (V_o) at 415 nm, 437 nm and 555 nm, respectively. Co-ZnO has two visible peaks along the 400 nm and 555 nm for valence band (VB) and V_o defects respectively. All the samples display the V_o and they range within 500-570 nm, which is the emission wavelength of green light [162].

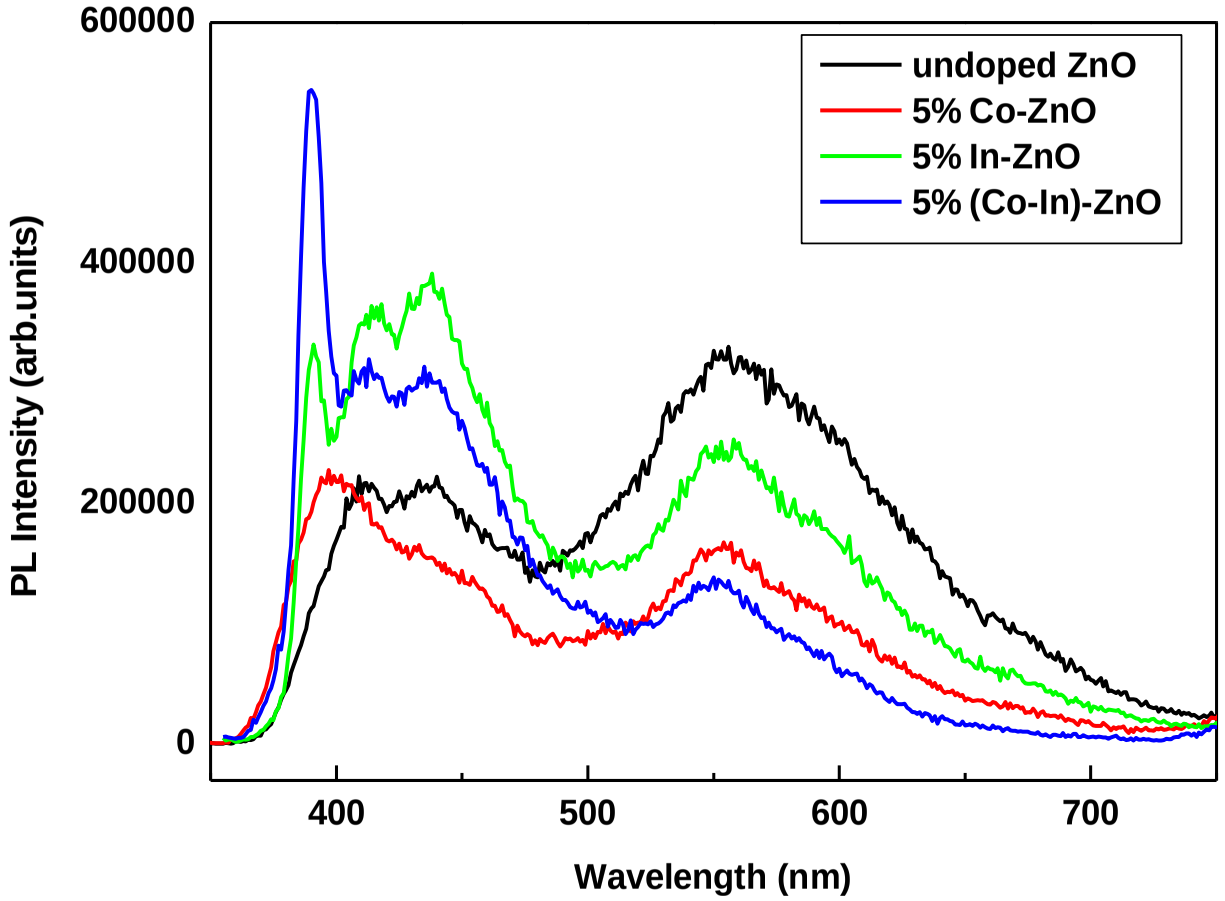

Figure 4.3.3: The Photoluminescence spectra for 5% doped and undoped ZnO nanoparticles at the excitation wavelength of 350 nm.

4.4 Conclusion

ZnO nanoparticles were successfully synthesised using high energy ball milling technique. The XRD characterisation confirms that the prepared samples were of hexagonal wurtzite ZnO nanoparticles. SEM images further validate the formation of spherical granular ZnO nanoparticles. The Raman spectra of the undoped ZnO nanoparticles displays a very strong peak of E_2 (high) that clearly indicate that the prepared material was of a hexagonal wurtzite ZnO phase. As the dopants were introduced in the ZnO nanostructure samples, a blue shift was experienced. The PL spectra indicated that doped ZnO nanoparticles have a strong UV emission peak at 380 nm and green emission band at 555 nm. Doped samples show very obvious peaks in the visible region of the spectrum. These peaks are an indication of defects in the original ZnO nanoparticles. From the UV-Vis results it can be concluded that as dopants are introduced into the ZnO structure the band gap decreases, which further decrease with co-doping the ZnO nanoparticles with Co-In.

Chapter 5

Gas sensing applications

5.1 Introduction

Over centuries various types of gas sensors such as the optical, electrochemical, catalytic acoustic and semiconductor have being developed [163]. The semiconducting metal oxide gas detectors such as SnO_2-ZnO [164], ZnO-CuO [165], Fe_2O_3-ZnO [166] have being investigated over a range of temperatures to detect most common gases [167], like H_2S, CO, NH_3, CH_4 and more to monitor the environment. Report by Feng et al. [168] indicated that enthanol (C_2H_5OH) gas is highly sensible and reflects fast response for ZnO-based sensors. The gas sensing properties of SnO_2 based sensors are found to be commonly influenced by the size and the Debye length of the polycrystalline SnO_2 particles [169]. Mean while, Wang et al. [170] investigations revealed that the gas sensing process depends mainly on the surface reaction where the chemical components, temperature, micro/nano-structure of the sensing layer and humidity play an important role.

H_2S is an acidic gas with the density slightly higher than that of air. It is known to have bad odor and is mostly present in industral areas, dumps and sewers. However, the monitoring of the H_2S gas is very important because it is dangerous to human health even at low concentrations [171]. It has being mentioned in several papers that the selectivity and sensitivity of gas sensors to H_2S can be improved through additives of hydrophobic silica [172], ceria or basic oxides to the sensing element and even doping with nobel metals like Ag to SnO_2 [173].

Tamaki et al. [169] reported on the extreme sensitivity of 5wt.% SnO_2-CuO to H_2S gas at 200^{o}C. The one dimensional metal oxide (nanobelt or nanowire based sensors) have

proved to possess numerous advantages, like higher sensitivity at parts-per-billion (ppb) and above, lower operating temperature and better compatibility compared to the traditional metal oxide sensors [174]. Wang et al. [175] further reported on the ZnO nanorods arrays prepared using a hydrothermal route for gas sensing application. In the report ZnO nanorods showed excellent response to NH_3 and CO exposure. Further on the H_2 gas sensitivity with detection limit of 20 ppm from room temperature to 250^oC was also observed. ZnO is known to be transparent to visible light and more electrically conductive through doping [176]. The n-type ZnO semiconductor occurs naturally, while the p-type ZnO semiconductor can be produced through co-doping techniques (N and Ga dopants) as indicated by Joseph et al. [177]. Amongst the high-performance gas sensing devices, ZnO nanorods have being found to be sensitive to gases such as H_2, NH_3 and C_2H_5OH at room temperature [178]. In this chapter , the undoped ZnO and (In or Co) single and (In and Co) double doped ZnO nanoparticles are subjected to NH_3, CH_4 and H_2S gases to check their sensitivity and selectivity.

5.2 Results and discussion

5.2.1 Ammonia (NH_3) gas

The ammonia (NH_3) gas sensing applications were performed for the undoped, Co and In single doped and Co and In double doped ZnO nanoparticles. These applications were performed at four temperatures: 200, 250, 300 and 350^oC. The response curves for NH_3 gas are plotted for different temperatures as shown in figure 5.2.1.1 below. It is observed that the undoped and double doped ZnO nanoparticles are favoured such that the In-ZnO and Co-ZnO nanoparticles are hardly visible. This may be due to the grain sizes of the undoped and (Co-In)-ZnO nanoparticles being smaller compared to those of In-ZnO and Co-ZnO nanoparticles. All the samples seem to show uneven pattern from 300^oC. Similar results were also obtained by Acuautla et al. [179] where a laser

ablation technique was used to manufacture ammonia gas sensing device which is ZnO nanoparticles based. This indicates that the NH_3 gas sensors performs badly at higher temperatures. In figure 5.2.1.1 (a) it has been noted that at 200^oC the current increases continuously without returning to the reference baseline as the gas concentration is increased.

In order to investigate the behaviour of sensitivity against concentration the equation: $S = \frac{R_{air}}{R_{NH_3}}$, was used. $R_{gas(NH3)}$ is the resistance in the presence of NH_3 gas at a given concentration and R_{air} is the resistance in the air environment. Now $R_{gas(NH3)}$ contributes 90 % of the response time, while R_{air} holds 10 % of the recovery time. The sensitivity of the undoped ZnO and (Co-In)-ZnO nanoparticles are constantly increasing with the increasing gas concentration, (see figure 5.2.1.2). In addition it is observed that the double doped ZnO exceeds the sensitivity of the undoped ZnO at 300^oC [91] and 350^oC. This is in good agreement with what Maswanganye et al. [91] obtained when testing NH_3 gas at 300^oC for (Co-In)-ZnO nanoparticles prepared by sol-gel method. Sensitivity of the undoped ZnO nanoparticles drops at 10 ppm but increases rapidly at 20 ppm to 100 ppm in figure 5.2.1.2 (a) and (b). In table 5.2.1, Co-ZnO nanoparticles show slow response time to NH_3 gas at 10 ppm but fast recovery time of 23 seconds. The Co-ZnO nanoparticles show a decrease in sensitivity as the gas concentration is increased in the temperature range 200-300^oC, thereafter experiences an increasing trend at 350^oC. The results suggest that the sensitivity of Co-ZnO nanoparticles is very poor at temperatures below 350^oC. In figure 5.2.1.2 (d) all the doped-ZnO nanoparticles samples display similar pattern of increase when the gas concentrations are increased. But it can be noted that the double doped ZnO nanoparticles is more sensitive compared to the single doped ZnO nanoparticles. In

general, all the samples show an enhanced sensitivity at 350^{o}C as shown in figure 5.2.1.2 (d).

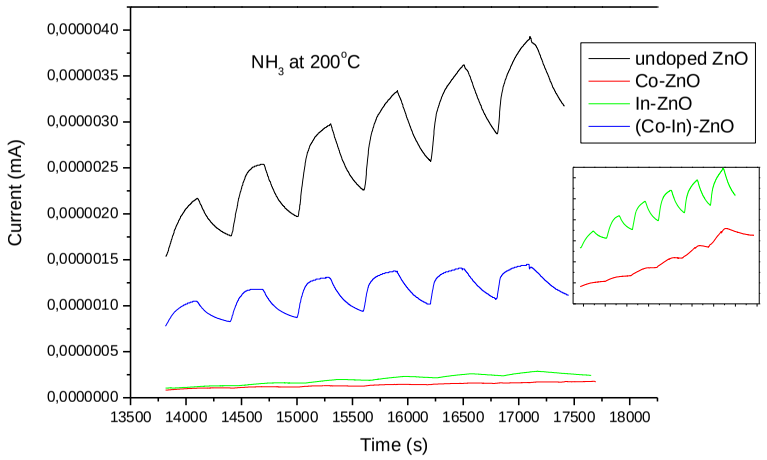

(a)

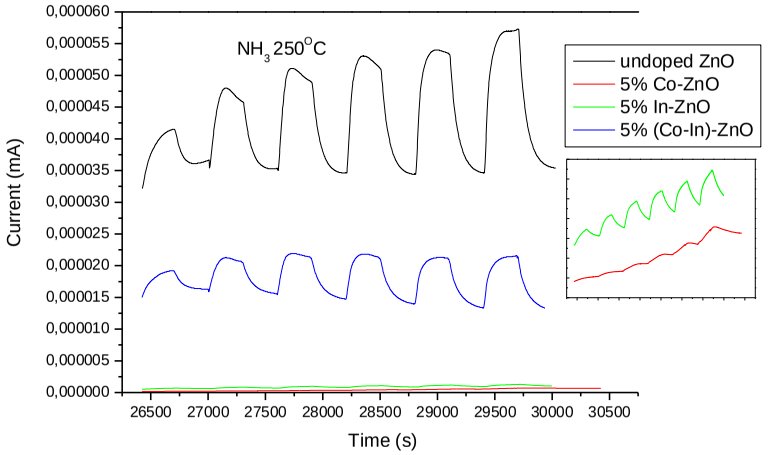

(b)

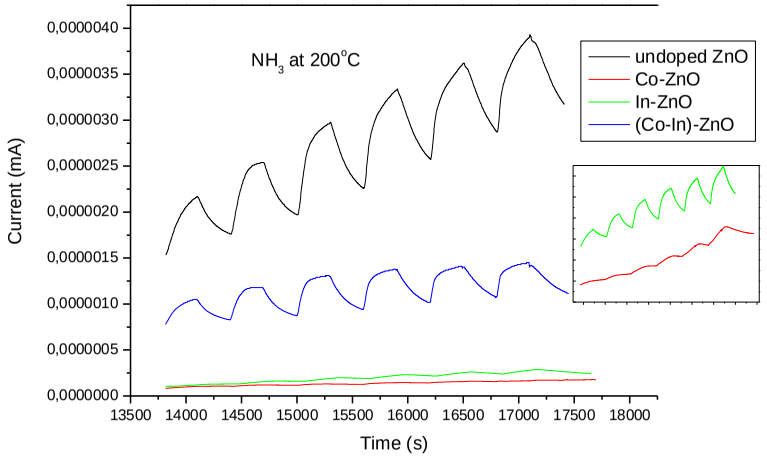

(c)

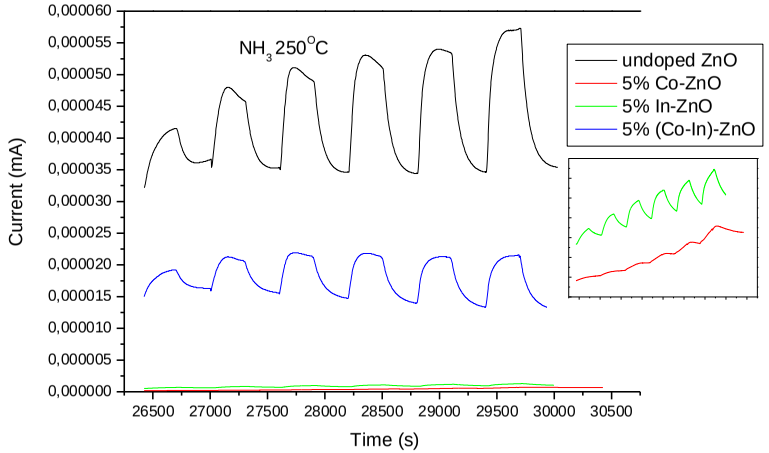

(d)

Figure 5.2.1. 1: The graphs of current against time for the doped and undoped ZnO nanoparticles at various temperatures for concentrations ranging between 5-100 ppm.

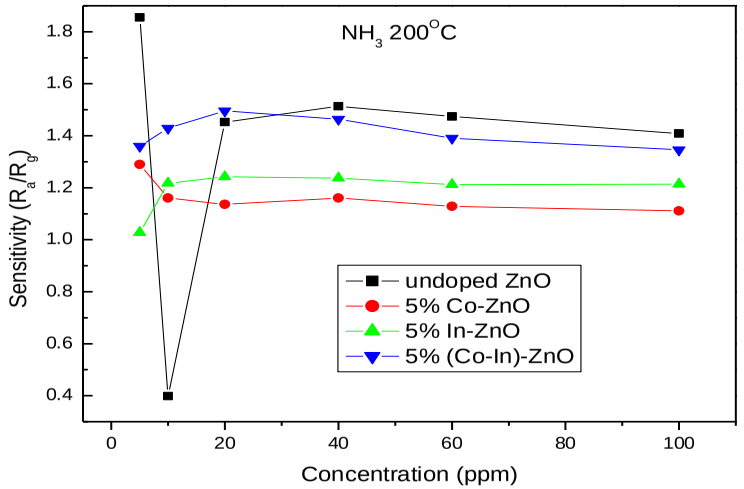

(a)

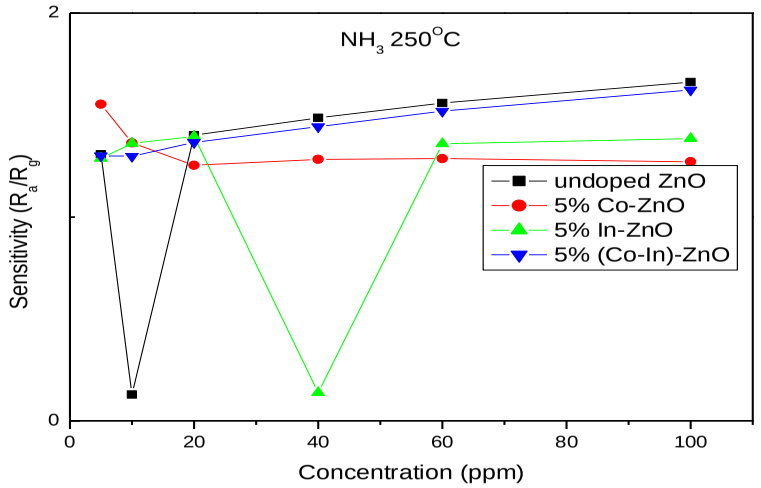

(b)

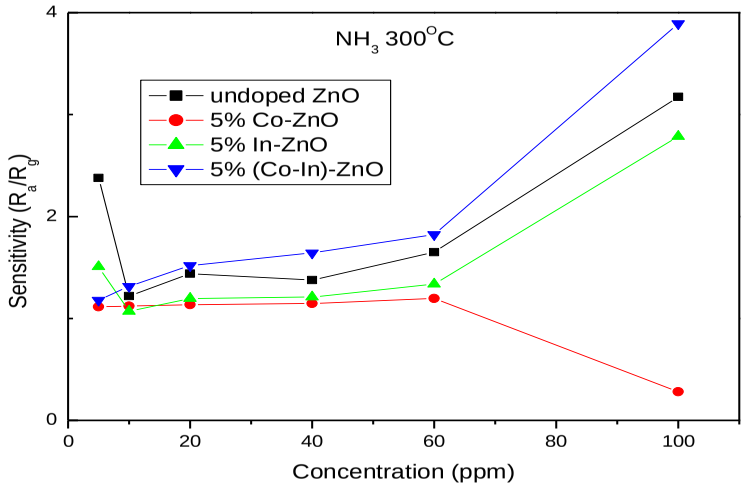

(c)

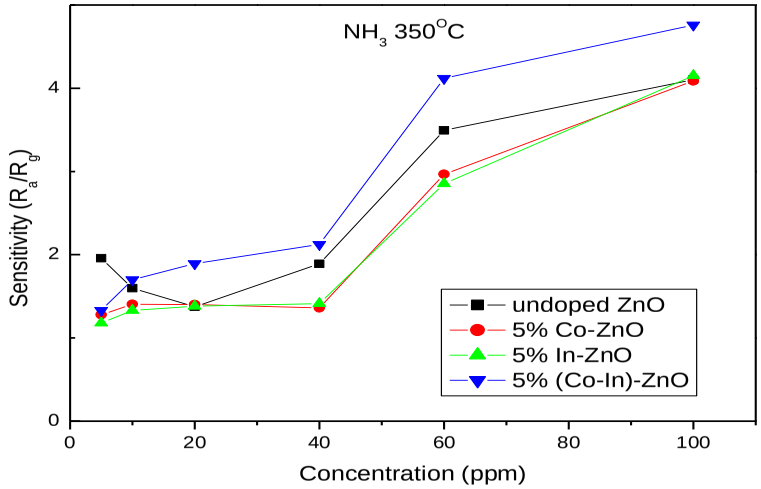

(d)

Figure 5.2.1. 2: The sensitivity versus NH_3 gas concentration plot for the doped and undoped ZnO nanoparticles.

5.2.2 Methane (CH_4) gas

The response curves for methane (CH_4) gas plotted in figure 5.2.2.1 below show that the prepared samples of undoped, single and double doped ZnO nanoparticles display good response at 200^oC. When the tempareture is elevated to temperatures above 250^oC, a poor response even with low CH_4 concentrations is observed. This means that the various ZnO nanoparticles samples operate very well at lower tempartures for CH_4 gas. Stolper et al. [180] reported that the thermogenic gases get produced in the temperature range of 157° to 221°C. This in turn also suggest that the sensors studied in this sub-section are good in this temperature range.

In figure 5.2.2.2 the undoped ZnO nanoparticles shows poor sensitivity of CH_4 gas through out all the tested temperatures. The double doped ZnO nanoparticles also reflect descending results in sensitivity when operating tempareture is increasing (200-350^oC). At 350^oC, all the samples reflect poor response at low concentrations (<40 ppm). The double doped ZnO nanoparticles sample seems to operate very well at 200^oC for the concentration of 40 ppm. The In-ZnO nanoparticles show high sensitivity at 20 ppm for 300^oC. In figure 5.2.2.2 (b)-(d) it is observed that Co-ZnO nanoparticles is the most sensitive to CH_4 gas, especially at 300^oC [181]. Motaung et al. [181] also observed similar results for ZnO nanostructures which were exposed to CH_4 concentrations at 300^oC for 24 hours.

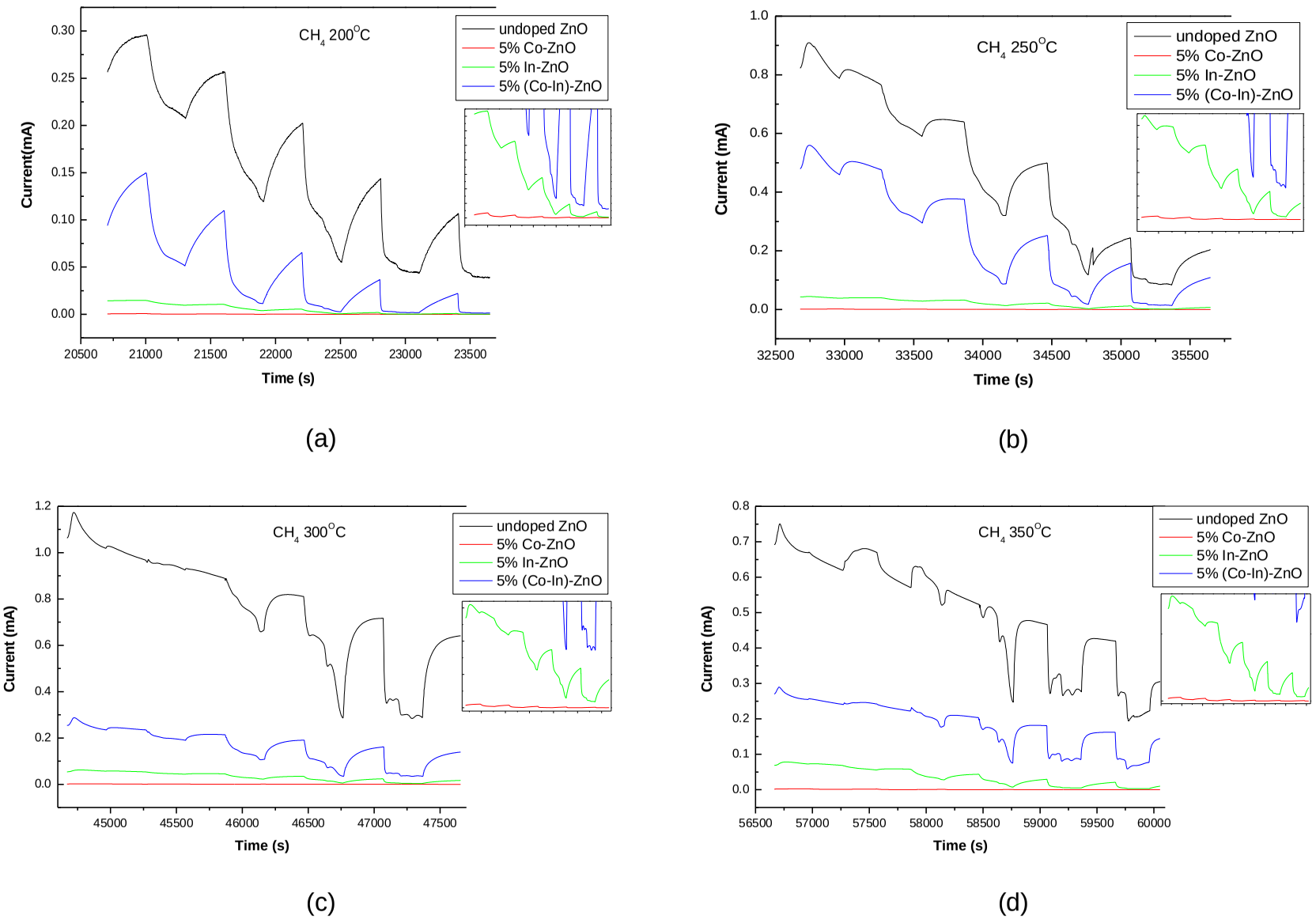

Figure 5.2.2. 1: The graphs of current against time for the doped and undoped ZnO nanoparticles at various temperatures for concentrations ranging between 5-100 ppm.

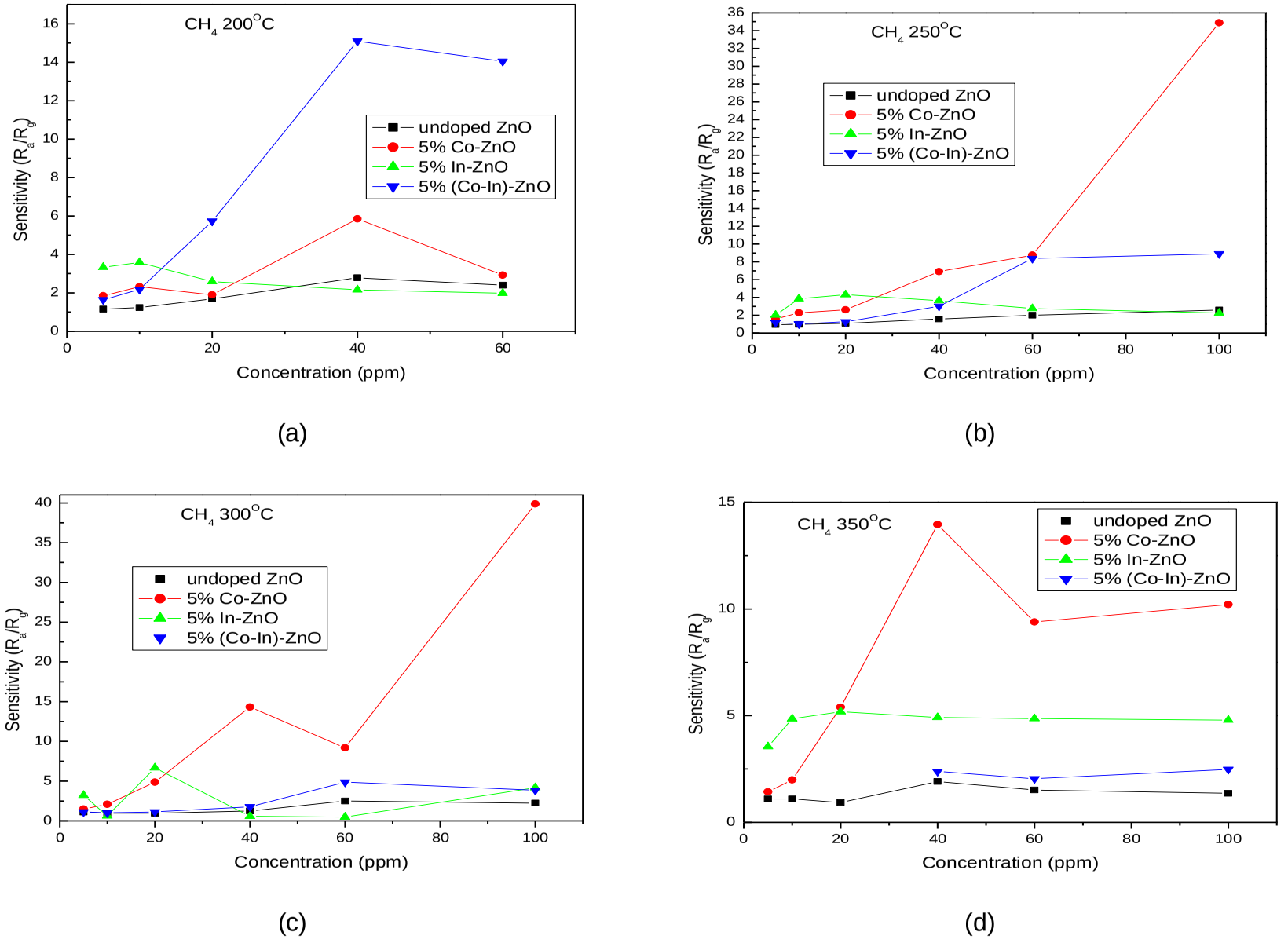

Figure 5.2.2. 2: The relationship between the sensitivity of the sensors and CH_4 gas concentrations at various temperatures.

5.2.3 Hydrogen sulphide (H_2S) gas

In the case of hydrogen sulphide (H_2S), the plot of response curves show an increase in sensitivity when the temperature and concentrations are increased for all the doped and undoped ZnO nanoparticles, (see figure 5.2.3.1). The undoped and double doped ZnO nanoparticles demonstrate the most dominant peaks. Moreover, when the tempareture is >200^oC the current remain constant for some time before it recovers. Making the peak flat at the top for higher concentrations of >40 ppm.

Like in the previous two sub-sections, figure 5.2.3.2 show the sensitivity plots against the H_2S gas concentrations for the undoped, (Co and In) single and double doped ZnO nanoparticles. The Co-ZnO nanoparticles are less sensitive amongst all the samples tested. Even at 350^oC it can be observed that the Co-ZnO nanoparticles sensitivity are decreasing as the gas concentrations are increased, while the sensitivity for undoped ZnO nanoparticles constantly increases with the increasing H_2S gas concentration. The double doped ZnO nanoparticles samples are the most sensitive to H_2S gas at 20 and 40 ppm for 300^oC and 350^oC, respectively [182]. In addition to what appears in figures 5.2.3.1 and 5.2.3.2, table 5.2.1 displays the response time for Co-ZnO nanoparticles as much slower compared to the recovery time. Meanwhile, the In-ZnO nanoparticles and double doped ZnO nanoparticles show equivalent time for both the response and recovery time. The sensitivity of In-ZnO nanoparticles is directly proportional to the gas concentrations at 200^oC and 250^oC [183]. Zeng et al. [184] reported on In_2O_3 nanowire gas sensors. In the study, he observed that In_2O_3 nanosensors are sensitive to H_2S gas both at room temperature and at 120^oC. The most outstanding results were obtained by Cuong et al. [185], where the ZnO nanorods on a chemically converted graphene film were found to detect 2 ppm of H_2S gas at room temperature.

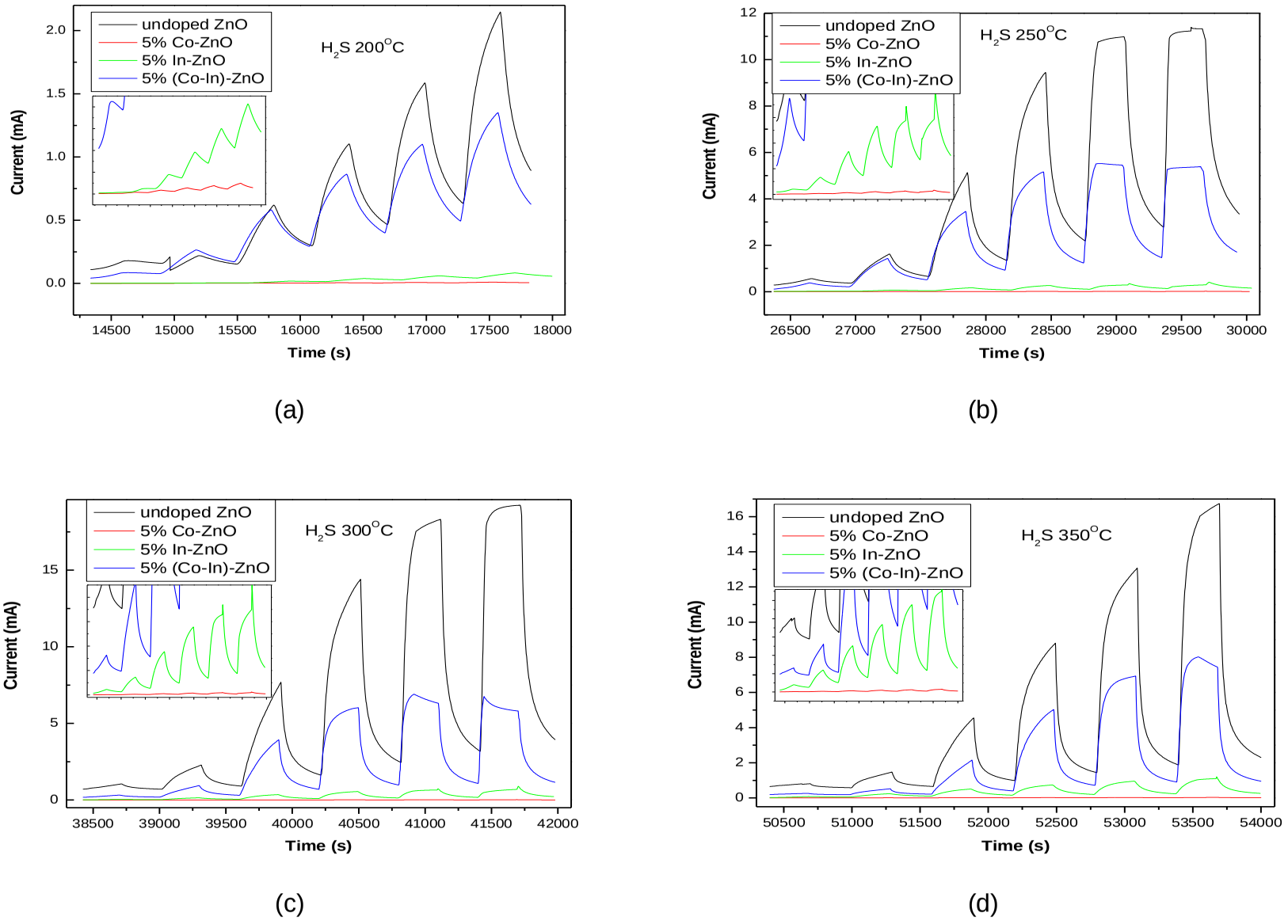

Figure 5.2.3. 1: The graphs of current against time for the doped and undoped ZnO nanoparticles at various temperatures for concentrations ranging between 5-100 ppm.

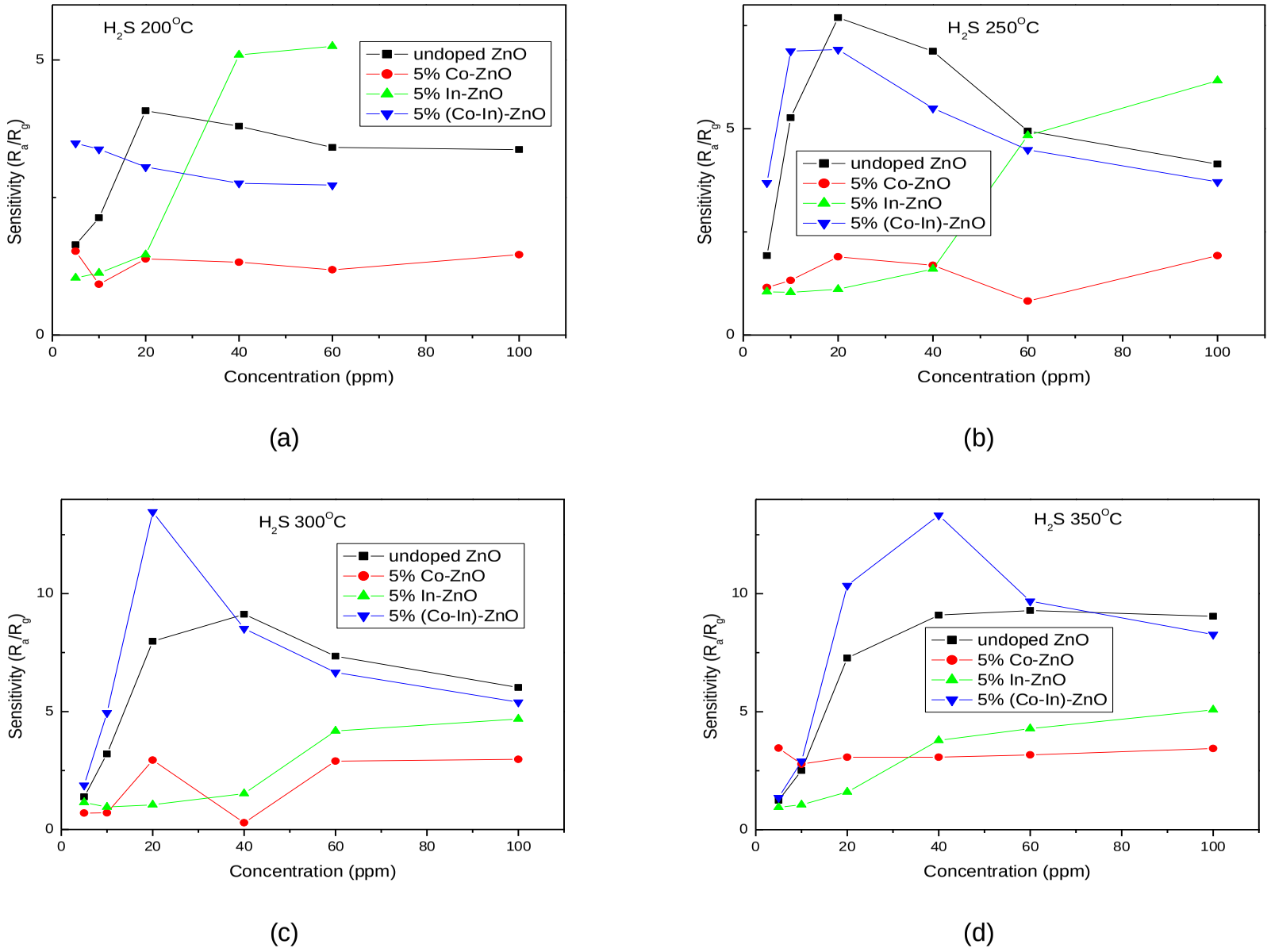

Figure 5.2.3. 2: The relationship between the sensitivity of the sensors and H_2S gas concentrations at various temperatures.

Table 5.2 1: The calculated results of response and recovery for the undoped ZnO, Co-ZnO, In-ZnO and (Co-In)-ZnO nanoparticles on NH_3, CH_4 and H_2S gases at 10 ppm exposed to 250^oC.

Sample	Gas	Response time (s)	Recovery time (s)
Undoped ZnO	NH_3	2.94×10^2	3.04×10^2
	CH_4	3.00×10^2	2.89×10^2
	H_2S	3.15×10^2	2.94×10^2
Co-ZnO	NH_3	5.72×10^2	2.30×10^1
	CH_4	2.99×10^2	3.00×10^2
	H_2S	3.01×10^2	2.89×10^2
In-ZnO	NH_3	3.02×10^2	3.02×10^2
	CH_4	2.98×10^2	2.97×10^2
	H_2S	2.82×10^2	3.24×10^2
(Co-In)-ZnO	NH_3	2.89×10^2	3.04×10^2
	CH_4	2.99×10^2	2.99×10^2
	H_2S	2.98×10^2	3.02×10^2

5.3 Conclusion

ZnO nanoparticles were successfully synthesized by the high energy ball milling technique. The undoped and (Co-In)-ZnO nanoparticles are more favored compared to the Co and In single doped ZnO nanoparticles. The current versus time curves are plotted for all the three gases: NH_3, CH_4 and H_2S, in which it can be observed that the double doped and undoped ZnO nanoparticles are dominating throughout the study. The NH_3 gas show good response and recovery at lower temperatures (< 250^oC), than at higher temperatures (> 250^oC). The Co-ZnO nanoparticles reflect an ascending response magnitude with increasing concentration of NH_3 gas, suggesting that the Co-ZnO nanoparticles performs better at higher temperature(< 350^oC). The CH_4 gas sensor seems to work better at lower temperatures and higher gas concentrations.

The double doped ZnO nanoparticles shows high CH_4 sensitivity at 200^oC which is good for monitoring the environment. The response curve for H_2S gas become smooth at the top as the temperature and concentration is increased. The double doped ZnO nanoparticles is most sensitive to 5 ppm at temperature range of 200-300^oC. In summary, the sensitivity is in the order of CH_4 > H_2S > NH_3 gas for all the tested temparetures. The current agianst time trend is in the order of H_2S > NH_3 > CH_4 gas for all the tested temperatures. The sesnitivity of the double doped ZnO nanoparticles reveals a good selectivity to CH_4 gas at low temperature and concentrations. Co-ZnO nanoparticles demonstrate favourable recovery time to NH_3 gas, but the double doped ZnO nanoparticles show minimal response and recovery time (2.99 $\times 10^2$ s) for CH_4 gas.

Chapter 6

Summary

In summary, the undoped, 5 % (In or Co) single and (In and Co) double doped ZnO nanoparticles have been successfully synthesised using the ball milling technique. The XRD characterisations were subsequently performed for all the prepared samples. The results showed that when the dopants are added on the undoped ZnO nanostructures, there is no significant effect (JCPDS No.36-1451). Only the In-ZnO nanoparticles display a new peak that is associated with the indium dopant. The new peak is attributed to the ionic radius of In^{3+} being larger compared to that of Zn^{2+} and also the preferred occupation site in the crystallite structure. In overall, this give the calculated crystallite size of the (Co-In)-ZnO nanoparticle as the smallest of all the prepared ZnO nanoparticles. The size effects can also be observed in the SEM images which demonstrate similarities in the morphology of the doped and undoped ZnO nanoparticles (more spherical).

Further investigations using the Raman spectroscopy were carried out and the well-known Raman modes for ZnO nanostructures were obtained. It can be observed from the Raman spectra that the undoped and In doped ZnO nanoparticles are favoured because of their high peak intensities. In addition, the A_1 and E_1 (LO) modes are being superimposed, making a broad peak. All the doped ZnO nanoparticles experience a blue-shift, which is in good agreement with the XRD patterns. The decrease in the energy band gaps of doped ZnO nanoparticles indicate that the introduction of (Co and In) dopants in the ZnO nanostructure can improve its performance such that the double doped ZnO nanoparticles have the lowest energy band gap. This results from the substitution of In^{3+} on the Zn^{2+} lattice site and some vacancies created during

doping process. In the PL study, the undoped ZnO nanoparticles revealed three types of vacancy defects [154]. Introduction of In and Co impurities influence the creation of intrinsic vacancies and interstitial type defects [154]. This is observed through an emerging peak from the double doped and In-ZnO nanoparticles spectra. Impurities further contribute to the decreased energy band gap in these doped nanoparticles.

The kenosistec station equipment was also used to probe the sensing properties of the doped and undoped ZnO nanoparticles to NH_3, CH_4 and H_2S gases. The double doped ZnO nanoparticles were found to be sensitive to CH_4 gas at low concentrations and low temperatures of 40 ppm and 200^oC, respectively. As the temperature is increased to 250^oC and above, the Co-ZnO nanoparticles acquire enhanced sensitivity to CH_4 gas. The NH_3 gas is best detected at 300 and 350^oC by the double doped ZnO nanoparticles, such that the sensitivity increases with the increasing concentrations. Good sensitivity to NH_3 gas were also observed at 350^oC for all the doped and undoped ZnO nanoparticles. The In doped ZnO nanoparticles were found to be sensitive to H_2S gas at 200^oC for 40 ppm. At higher temperatures the double doped ZnO nanoparticles show an enhanced sensitivity to the H_2S gas even at low concentrations (<40 ppm). The results also show that the double doped ZnO nanoparticles has low resistance to current as such is sensitive at much lower temperatures compared to the single doped ZnO nanoparticles. It can also be seen that the sensitivity is more related to conductivity of these nanoparticles.

7. Reference

[1] T. N. Soitah, Y. Chunhui and S. Liang, “Effect of Fe doping on structural and electrical properties of nanocrystalline ZnO thin films prepared by sol–gel dip coating technique,” *Science of Advanced Materials,* vol. 2, p. 534–538, 2010.

[2] L. Pueyo, S. Siroky, S. Landsmann, M. E. V. D Berg, M. R. Wagner, J. S. Reparaz, A.Hoffmann and S. Polarz, “Molecular precursor route to a metastable form of Zinc Oxide,” *Chemistry of Materials,* vol. 22, p. 4263–4270, 2010.

[3] Ü. Özgür, Ya. I. Alivov, C. Liu, A. Teke, M. A. Reshchikov, S. Doğan, V. Avrutin, S. -J. Cho and H. Morkoç, “A comprehensive review of ZnO materials and devices,” *Journal of Applied Physics,* vol. 98, pp. 041301-0413103, 2005.

[4] B. M. Rajbongshi and S. K. Samdarshi, “Cobalt-doped zincblende-wurtzite mixed-phase ZnO photocatalyst nanoparticles with high activity in visible spectrum,” *Applied Catalysis B: Enviromental,* vol. 144, pp. 435-441, 2014.

[5] V. Eskizeybek, F. Sarı, H. Gülce, A. Gülce and A. Avcı, “Preparation of the new polyaniline/ZnO nanocomposite and its photocatalytic activity for degradation of methylene blue and malachite green dyes under UV and natural sun lights irradiations,” *Applied Catalysis B: Environ-mental,* vol. 119–120, p. 197–206, 2012.

[6] Z. L. Wang, “Zinc oxide nanostructures: growth, properties and applications,” *Journal of physics: condensed matter,* vol. 16, p. 829–858, 2004.

[7] W. Hsuan-Chung, P. Yen-Chun and S. Tsu-Ping, “Electronic and Optical Properties of Substitutional and Interstitial Si-Doped ZnO,” *Materials,* vol. 5, pp. 2088-2100, 2012.

[8] Y. Zhang and J. Mu, “Controllable synthesis of flower-and rod-like ZnO nanostructures by simply tuning the ratio of sodium hydroxide to zinc acetate,” *Nanotechnology,* vol. 18, p. 075606, 2007.

[9] Q. Zhang, C. S. Dandeneau, X. Zhou and G. Cao, “ZnO nanostructures for dye-sensitized solar cells,” *Advanced Mater,* vol. 21, pp. 4087-4108, 2009.

[10] M. Ramani, S. Ponnusamy, C. Muthamizhchelvan, J. Cullen, S. Krishnamurthy and E. Marsili, “Morphology-directed synthesis of ZnO nanostructures and their antibacterial activity,” *Colloids Surf B Biointerface,* vol. 105, pp. 24-30, 2013.

[11] A. Top and H. Çetinkaya, “Zinc oxide and zinc hydroxide formation via aqueous precipitation: Effect of the preparation route and lysozyme addition,” *Materials Chemistry and Physics,* vol. 167, p. 77–87, 2015.

[12] T. Prakash, R. Jayaprakash, D. S. Raj, S. Kumar, N. Donato, D. Spadaro and G. Neri, “Sensing properties of ZnO nanoparticles synthesized by using albumen as a biotemplate for acetic acid monitoring in aqueous mixture,” *Sensors and Actuators B: Chemical,* vol. 176, p. 560– 568, 2013.

[13] Z. Fan and J. G. Lu, “Zinc Oxide Nanostructures: Synthesis and Properties,” *Journal of Nanoscience and Nanotechnology,* vol. 5, pp. 1-28, 2005.

[14] I. Djerdj, G. Garnweitner, D. Arcon, M. Pregelj, Z. Jaglicic and M. Niederberger, “Diluted Magnetic Semiconductors: Mn/Co-Doped ZnO Nanorods,” *Materials Chemistry,* vol. 18, pp. 5208-5217, 2008.

[15] R. A. Buhrman and C. G. Granqvist, “Log-normal size distributions from magnetization measurements on small superconducting Al particles,” *Applied Physics,* vol. 47, pp. 2220-2222, 1976.

[16] T. Kodas, “Aerosol Spray Pyrolysis Synthesis Techniques,” *Advanced Materials,* vol. 6, pp. 180-192, 1989.

[17] S. Indris, D. Bork and P. Heitjans, “Nanocrystalline Oxide Ceramics Prepared by High-Energy Ball Milling,” *Materials Synthesis and Processing,* vol. 8, pp. 245-250, 2000.

[18] L. Xu, Y. Su, Y. Chen, H. Xiao, L. A. Zhu, Q. Zhou and S. Li, “Synthesis and characterization of indium-doped ZnO nanowires with periodical single-twin structures,” *Journal of Physical Chemistry B,* vol. 110, p. 6637–6642, 2006.

[19] Y. Z. Zheng, X. Tao, Q. Hou, D. T. Wang, W. L. Zhou and J. F. Chen, “Metal and F Dual-doping to Synchronously Improve Electronic Transport Rate and Lifetime for TiO2 Photoanode to Enhance Dye-Sensitized Solar Cells Performances,” *Materials Chemistry A,* vol. 23, pp. 3-5, 2010.

[20] S. K. Kim, S. Y. Jeong and C. R. Cho, “Structural reconstruction of hexagonal to cubic ZnO films on Pt/Ti/SiO2/Si substrate by annealing,” *Applied Physics Letters,* vol. 82, pp. 562-565, 2003.

[21] A. Sudha, S. L. Sharma and T. K. Maity, “Effects of annealing temperature on structural and electrical properties of indium oxide thin films prepared by thermal evaporation,” *Materials letters,* vol. 157, pp. 19-22, 2015.

[22] D. Sharma, S. Sharma, B. S. Kaith, J. Rajput and M. Kaur, “Synthesis of ZnO nanoparticles using surfactant free in-air and microwave method,” *Applied Surface Science,* vol. 257, p. 9661–9672, 2011.

[23] K. Ihokura and J. Watson, “Characteristics of Nanoparticles-Based Chemical Sensors,” *Materials Sciences and Applications,* vol. 3, pp. 448-452, 2012.

[24] B. P. L. Costello, R. J. Ewen, N. Guernion and N. M. Ractlife, “Highly Sensitive Mixed Oxide Sensors for the Detection of Ethanol,” *Sensors and Actuators B,* vol. 87, pp. 207-210, 2002.

[25] L. M. Fang, X. T. Zu, Z. J. Li, S. Zhu, C. M. Liu, W. L. Zhou, L. M. Wang and J. Alloys, “Synthesis and characteristics of Fe3+-doped SnO2 nanoparticles via sol–gel-calcination or sol–gel-hydrothermal route,” *Journal of Alloys and Compounds,* vol. 454, p. 261–267, 2008.

[26] S. J. Pearton, D. P. Norton, M. P. Mil, A. F. Hebard, J. M. Zavada, W. M. Chen and I. A. Buyanova, “ZnO Doped with Transition Metal Ions,” *IEEE Transactions on Electron Devices,* vol. 54, pp. 1040-1048, 2007.

[27] T. Yu-Feng, H. Shu-Jun, Y. Shi-Shen and M. Liang-Mo, “Oxide magnetic semiconductors: Materials, properties, and devices,” *Chinese Physics B,* vol. 22, p. 088505, 2013.

[28] D. H. Kim, N. G. Cho, H. G. Kim, W. Choib, “Structural and Electrical Properties of Indium Doped ZnO Thin Films Fabricated by RF Magnetron Sputtering,” *Journal of The Electrochemical Society,* vol. 154, pp. H939-H943, 2007.

[29] N. L. Tarwal, K. V. Gurav, S. H. Mujawar, J. H. Jang, J. H. Kim, “Photoluminescence and photoelectrochemical properties of the spray deposited copper doped zinc oxide thin films,” *Ceramics International,* vol. 40, pp. 7669-7677, 2014.

[30] M. S. Hassan, T. Amna, O. Yang, H. Kim, M. Khil, “TiO2 nanofibers doped with rare earth element and their photocatalytic activity,” *Ceramics International,* vol. 38, p. 5925–5930, 2012.

[31] S. Anandan, A. Vinu, T. Mori, N. Gokulakrishnan, P. Srinivasu, V. Murugesan and K. Ariga, “Photocatalytic degradation of 2,4,6-triclorophenol using lanthanum doped ZnO in aqueous suspension,” *Catalysis Communication,* vol. 8, p. 1377–1382, 2007.

[32] Y. Chang, J. Xu, Y. Zhang, S. Ma, L. Xin, L. Zhu and C. Xu, “Optical Properties and Photocatalytic Performances of Pd Modified ZnO Samples,” *Journal of Physical Chemistry C,* vol. 113, p. 18761–18767, 2009.

[33] R. S. Razavi, M. R. Loghman-Estarki, M. Farhadi-Khouzani, M. Barekat and H. Jamali, “Large Scale Synthesis of Zinc Oxide Nano- and Submicro-Structures by Pechini's,” *Current Nanoscience,* vol. 7, pp. 807-812, 2011.

[34] N. Kiomarsipourn and R. S. Razavi, “Hydrothermal synthesis of ZnO nanopigments with high UV absorption and vis/NIR reflectance,” *Ceramics International,* vol. 40, p. 11261–11268, 2014.

[35] X. U. Dong, T. Dong-mei, J. Lei, “Effects of high-energy ball milling oxide-doped and varistor ceramic powder on ZnO varistor,” *Transactions of Nonferrous Metals Socirty of China,* vol. 22, p. 1423−1431, 2012.

[36] M. H. Huang, Y. Wu, H. Feick, N. Tran, E. Weber and P. Yang, “Catalytic growth of zinc oxide nanowires by vapor transport,” *Advanced Materials,* vol. 13, pp. 113-116, 2001.

[37] P. P. Ahonen, J. Joutsensaari and O. Richard, “Mobility size development and the crystallization path during aerosol decomposition synthesis of TiO2 particles,” *Journal of Aerosol Science,* vol. 32, pp. 615-630, 2001.

[38] M. L. Ostraat, J. W. De-Blauwe, M. L. Green, L. D. Bell, H. A. Atwater and R. C. Flagan, “Ultraclean two-stage aerosol reactor for production of oxide-passivated silicon nanoparticles for novel memory devices,” *Journal of Electrochem Society,* vol. 148, pp. G265-G270, 2001.

[39] S. D. Charpe, F. C. Raghuwanshi, G. T. Lamdhade and V. S. Kalymwar, “Synthesis of Nano structure Zinc Oxide by Spray Pyrolysis and its

Characterizationfor Gas Sensing Application," *IPASJ International Journal of Electrical Engineering,* vol. 3, pp. 12-17, 2015.

[40] H. C. Cheng, C. F. Chen and C. C. Lee, "Thin-film transistors with active layers of zinc oxide (ZnO)," *Thin Solid Films ,* vol. 498, p. 142 – 145, 2006.

[41] V. Gandhi, R. Ganesan, H. H. A. Syedahamed and M. Thaiyan, "Effect of cobalt dopingon structural, optical, and magnetic properties of ZnO nanoparticles synthe-sized by coprecipitation method," *Journal of Physical Chemistry C,* vol. 118, p. 9715–9725, 2014.

[42] D. P. Norton, M. E. Overberg, S. J. Pearton, K. Pruessner, J. D. Budai, L. A. Boatner,M. F. Chisholm, J. S. Lee, Z. G. Khim, Y. D. Park and R. G. Wilson, "Ferromagnetism in cobalt-implanted ZnO," *Applied Physics Letters,* vol. 83, p. 5488–5490, 2003.

[43] K. Rode, A. Anane, R. Mattana, J.P. Contour, O. Durand and R.L. Bourgeois, "Magnetic semiconductors based on cobalt substituted ZnO," *Journal of Applied Physics,* vol. 93, pp. 7676-7678, 2003.

[44] N. Karak, B. Pal, D. Sarkar and T. K. Kundu, "Grow of Co-doped ZnO nanoparticles by porous alumina assisted sol-gel route: Structural optical and magnetic properties," *Journal of Alloys and Compounds,* vol. 647, pp. 252-258, 2015.

[45] H. Yang and S. Nie, "Preparation and characterization of Co-doped ZnO nanomaterials," *Materials Chemistry and Physics ,* vol. 114, p. 279–282, 2009.

[46] P. N. Lisboa-Filho, C. Vila, M. S. Góes, C. Morilla-Santos, L. Gama, E. Longo, W. H. Schreiner and C. O. Paiva-Santos, “Composition and electronic structure of Zn7−xMxSb2O12 (M = Ni and Co) spinel compounds,” *Materials Chemistry and Physics,* vol. 85, p. 377–382, 2004.

[47] C. J. Cong, L. Liao, J. C. Li, L.X. Fan-dan and K. L. Zhang, “Synthesis, structure and ferromagnetic properties of Mn-doped ZnO nanoparticles,” *Nanotechnology,* vol. 16, p. 981–984, 2005.

[48] M. El-Hilo and A. A. Dakhel, “Structural and magnetic properties of Mn-doped ZnO powders,” *Journal of Magnetism and Magnetic Materials,* vol. 323, p. 2202–2205, 2011.

[49] R. Lamba, A. Umar, S. K. Mehta and S. K. Kansal, “ZnO doped SnO2 nanoparticles heterojunction photo-catalyst for environmental remediation,” *Journal of Alloys and Compounds,* vol. 653, pp. 327-333, 2015.

[50] Z. L. Wang, “Nanostructures,” *Materials today,* vol. ISSN:1369 7021, pp. 26-33, 2004.

[51] S. Baruah and J. Dutta, “Hydrothermal growth of ZnO nanostructures,” *Science and Technology of Advanced Materials,* vol. 10, pp. 013001-0130019, 2009.

[52] J. Serrano, A. H. Romero, F. J. Manjo´n, R. Lauck, M. Cardona and A. Rubio, “Pressure dependence of the lattice dynamics of ZnO: An ab initio approach,” *Physical Review B,* vol. 69, pp. 0943061-09430614, 2004.

[53] J. L. MacManus-Driscoll and L. Schmidt-Mende , “ZnO- nanostructure, defects, and devices,” *Materials today,* vol. 10, pp. 40-48, 2007.

[54] S. B. Zhang, S. H. Wei and A. Zunge, “Intrinsic n-type versus p-type doping asymmetry and the defect physics of ZnO,” *Physical Review B,* vol. 63, pp. 0752051-0752057, 2001.

[55] H. Kato, M. Sano, K. Miyamoto and T. Yao, “Growth and characterization of Ga-doped ZnO layers on a-plane sapphire substrates grown by molecular beam epitaxy,” *Journal of Crystal Growth,* vol. 237–239, p. 538–543, 2002.

[56] Z. L. Wang, “Zinc oxide nanostructures: growth, properties and applications,” *Journal of Physics: Condensed Matter,* vol. 16, p. R829–R858, 2004.

[57] H. Iwanaga , M. Fujii and S. Takeuchi, “Growth model of tetrapod zinc oxide particles,” *Journal of Crystal Growth,* vol. 134, pp. 275-280, 1993.

[58] O. Dulub, L. A. Boatner, U. Diebold, “STM study of the geometric and electronic structure of ZnO(0001)-Zn, (000-1)-O, (10-10), and (11-20) surfaces,” *Surface Science,* vol. 519, pp. 201-217, 2002.

[59] R. M. Martin, “Relation between Elastic Tensors of Wurtzite and Zinc-Blende Structure Materials,” *Physical Review 8,* vol. 6, pp. 4546- 4553, 1972.

[60] A. Ashrafi and C. Jagadish, “Review of zincblende ZnO: Stability of metastable ZnO phases,” *Journal of Applied Physics,* vol. 102, p. 071101, 2007.

[61] J.A. Sans, A. Segura, F.J. Manjo´n, B. Marı, A. Munoz and M.J. Herrera-Cabrera , “Optical properties of wurtzite and rock-salt ZnO under pressure,” *Microelectronics Journal ,* vol. 36, p. 928–932, 2005.

[62] A. Schleife, F. Fuchs, J. Furthmüller and F. Bechstedt, “First-principles study of ground- and excited-state properties of MgO, ZnO and CdO polymorphs,” *Physics Review B,* vol. 73, pp. 2452121-24521214, 2006.

[63] H. Dixit, R. Saniz, D. Lamoen and B. Partoens, “The quasiparticle band structure of zincblende and rocksalt ZnO,” *Journal of Physics: Condensed Matter,* vol. 22, pp. 125505-1255011, 2010.

[64] J. E. Jaffe, J. A. Snyder, Z. Lin, and A. C. Hess, “LDA and GGA calculations for high-pressure phase transitions in ZnO and MgO,” *Physics Review B: Condensed Matter Material Physics,* vol. 62, pp. 1660-1665, 2000.

[65] Y. Saeed, A. Shaukat, N. Ikram and M. Tanveer, “Structural and Electronic Properties of Rock Salt Phase of ZnO under Compression,” *Journal of Physical Chemistry of Solids,* vol. 69, p. 1676−1683, 2008.

[66] A. N. Baranov, P. S. Sokolov, V. A. Tafeenko, C. Lathe, Y.V. Zubavichus, A. A. Veligzhanin, M. V. Chukichevand V. L. Solozhenko, “Nanocrystallinity as a Route to Metastable Phases: Rock Salt ZnO,” *Chemistry of Material,* vol. 25, p. 1775−1782, 2013.

[67] A. Duzynska, R. Hrubiak, V. Drozd, H. Teisseyre, W. Paszkowicz, A. Reszka, A. Kaminska, S. Saxena, J. D. Fidelus and J. Grabis, “The Structural and

Optical Properties of ZnO Bulk and Nanocrystals under High Pressure.," *High Pressure Research,* vol. 32, p. 354−363, 2012.

[68] Y. Zhang, Z. Gao and Y. Gu,, "First-Principles Studies on the Structural Transition of ZnO Nanowires at High Pressure," *Journal of Nanomaterials,* vol. 2010, pp. 462032- 462037, 2010.

[69] Y. Wang, T. Hou, S.Tian, S. Lee and Y. Li, "Influence of doping effect on zinc oxide by first-principles studies," *Journal of Physical Chemistry C,* vol. 115, p. 7706−7716, 2011.

[70] Y. Ding and Z. L. Wanga, "Zinc-blende ZnO and its role in nucleating wurtzite tetrapods and twinned nanowires," *Applied Physics Letters,* vol. 90, pp. 153511- 153513, 2007.

[71] P. Y. Yu and M. Cardona, "Fundamentals of Semiconductors- Physics and Materials Properties," *2nd edition, Springer, Berlin,* 1999.

[72] M. Willander, O. Nur, J. R. Sadaf, M. I. Qadir, S. Zaman, A. Zainelabdin, N. Bano and I. Hussain, "Luminescence from Zinc Oxide Nanostructures and Polymers and their Hybrid Devices," *Materials,* vol. 3, pp. 2643-2667, 2010.

[73] P. BarnitA, S. Budhi, G. Subhasis and R. Anushree, "A comparative study on electrical and optical properties of group III (Al, Ga, In) doped ZnO," *Thin Solid Films,* vol. 603, p. 21–28, 2016.

[74] A. Janotti and C. G. Van de Walle, "Fundamentals of zinc oxide as a semiconductor," *Reports on Progress in Physics,* vol. 72, pp. 126501-126529, 2009.

[75] B. L. Zhu, C. S. Xie, J. Wu, D. W. Zeng, A. H. Wang and X. Z. Zhao, “Influence of Sb, In and Bi dopants on the response of ZnO thick films to VOCs,” *Materials Chemistry and Physics,* vol. 96, p. 459–465, 2006.

[76] Y. S. Wang, P. John Thomas and P. O’Brien, “Optical Properties of ZnO Nanocrystals Doped with Cd, Mg, Mn, and Fe Ions,” *Journal of Physical Chemistry B,* vol. 110, pp. 21412-21415, 2006.

[77] M. Wang , E. K. Na, J. S. Kim , E. J. Kim , S. H. Hahn , C.Park and K. Koo, “Photoluminescence of ZnO nanoparticles Prepared by low-temperature colloidal chemistry method,” *Materials Letters,* vol. 61, pp. 4094-4096, 2007.

[78] A. Rahmati, A. B. Sirgani, M. Molaei, and M. Karimipour, “Cu-doped ZnO nanoparticles synthesized by simple co-precipitation route,” *The European Physical Journal Plus,* vol. 129: 250, pp. 2-7, 2014.

[79] T. L. Tan, C. W. Lai, and S. B. A. Hamid, “Tunable Band Gap Energy of Mn-Doped ZnO Nanoparticles Using the Coprecipitation Technique,” *Journal of Nanomaterials,* vol. 2014, p. 371720, 2014.

[80] T. Prasada Rao, M.C. Santhoshkumar, “Effect of thickness on structural, optical and electrical properties of nanostructured ZnO thin films by spray pyrolysis,” *Applied Surface Science,* vol. 225, p. 4579–4584, 2009.

[81] J. Mizsei, “How can sensitive and selective semiconductor gas sensors be made?,” *Sensors and Actuators B,* vol. 23, pp. 173-176, 1995.

[82] B. K Meyer, H. Alves, D.M. Hofmann, W. Kriegseis, D. Forster, F. Bertram, J. Christen, A. Hoffmann, M. Straßburg, M. Dworzak, U. Haboeck and A. V.

Rodina, “Bound exciton and donor–acceptor pair recombinations in ZnO,” *Physics Status Solidi (b),* vol. 241, p. 231–260, 2004.

[83] M. Ferhat, A. Zaoui and R. Ahuja, “Magnetism and band gap narrowing in Cu-doped ZnO,” *Applied Physics Letters,* vol. 94, pp. 142502-142505, 2009.

[84] H. Jr. He, T. H. Wu, C. L. Hsin, K. M. Li, L. J. Chen, Y. L. Chueh, L. J. Chou and Z. L. Wang, “Beaklike SnO2 Nanorods with Strong Photoluminescent and Field-Emission Properties,” *General Nanotechnology,* vol. 2, pp. 116-120, 2006.

[85] A. Walsh, J. L. D. Silva, S. -H. Wei, C. Körber, A. Klein, L. F. Piper, A. DeMasi, K. E. Smith, G. Panaccione, P. Torelli, D. J. Payne, A. Bourlange and R. G. Egdell, “The nature of the bandgap in In2O3 revealed by first-principles calculations and X-ray spectroscopy,” *Physical Review Letters,* vol. 100, pp. 167402-167404, 2008.

[86] L. Holland and G. Siddall, “Heat-reflecting windows using gold and bismuth oxide films,” *British Journal of Applied Physics,* vol. 9, p. 375–391, 1958.

[87] R. Groth and E. Kauer, “Low-pressure sodium lamps with indium oxide filter,” *Philips Technical Review 26,* vol. 26, pp. 105- 111, 1965.

[88] N. K. Seng, M. K. Ahmad, N. S. Jasmin, N. B. Zainal, N. Nayan, S. C. Fhong, A. B. Suriani and A. Mohamed, “Effect of annealing time on aluminium doped tin oxide (SnO2) as a transparent conductive oxide,” *ARPN Journal of Engineering and Applied Sciences,* vol. 11, pp. 8915-8920, 2016.

[89] P. D. C. King, T. D. Veal, F. Fuchs, Ch. Y. Wang, D. J. Payne, A. Bourlange, H. Zhang, G. R. Bell, V. Cimalla, O. Ambacher, R. G. Egdell, F. Bechstedt and C. F. McConville, “Band gap, electronic structure, and surface electron accumulation of cubic and rhombohedral In2O3,” *Physical Review B,* vol. 79, pp. 205211-205221, 2009.

[90] B. L'Azou, I. Passagne, S. Mounicou, M. Tréguer-Delapierre, I. Puljalté, J. Szpunar, R. Lobinskib and C. Ohayon-Courtès, “Comparative cytotoxicity of cadmium forms (CdCl2, CdO, CdS micro- and nanoparticles) in renal cells,” *Toxicology Research,* vol. 3, pp. 32-41, 2014.

[91] M. W. Maswanganye, K. E. Rammutla, T. E. Mosuang and B. W Mwakinkunga, “The effect of Co and In combinational or individual doping on the structural, optical and selective properties of ZnO nanoparticles,” *Sensors and Actuators B,* vol. 247, pp. 228-237, 2017.

[92] A. Gurlo, “Nanosensors: Towards morphological control of gas sensing activity. SnO2, In2O3, ZnO and WO3 case studies,” *Nanoscale,* vol. 3, p. 154–165, 2011.

[93] J. Robertson and B. Falabretti, “Electronic Structure of Transparent Conducting Oxides,” in *Department of Engineering, Cambridge University*, UK, Cambridge CB2 1PZ, 2011, pp. 27-50.

[94] H. Odaka, S. Iwata, N. Taga, S. Ohnishi, Y. Kaneta, Y. Shigesato, “Electronic Structures and Optical Properties of ZnO, SnO2 and In2O3,” *Japanese Journal of Applied Physics,* vol. 38, p. 3453–3458, 1999.

[95] H. Hosono, “Ionic amorphous oxide semiconductors: Material design, carrier transport, and device application,” *Journal of Non-Crystalline Solids,* vol. 352, p. 851–858, 2006.

[96] P. G. Patil, D. D. Kajale, V. P. Patil, G. E. Patil and G. H. Jain, “synthesis of nanostructured zro2 for gas sensing application,” *International Journal on Smart Sensing and Intelligent Systems,* vol. 5, pp. 673-684, 2012.

[97] P. Duy-Thach and C. Gwiy-Sang, “Effects of defects in Ga-doped ZnO nanorods formed by a hydrothermal method,” *Sensors and Actuators B: Chemical,* vol. 187, p. 191–197, 2013.

[98] A. Rim-Rukeh, “An assessment of the contribution of municipaal solid waste dump site fire to atmospheric pollution,” *Open Journal of Air Pollution,* vol. 3, pp. 53-60, 2014.

[99] G. Korotcenkov, S. D. Han and J. R. Stetter, “Review of electrochemical hydrogen sensors,” *Chemical Reviews,* vol. 109, pp. 1402-1433, 2009.

[100] M. Momirlan and T. N. Veziroglu, “The properties of hydrogen as fuel tomorrow in sustainable energy system for a cleaner planet,” *International Journal of Hydrogen Energy,* vol. 30, pp. 795-802, 2005.

[101] H. Gong , J.Q. Hu, J.H. Wang, C.H. Ong and F.R. Zhu, “Nano-crystalline Cu-doped ZnO thin film gas sensor for CO,” *Sensors and Actuators B,* vol. 115, p. 247–251, 2006.

[102] J. Q. Xu, X. H. Wang and J. N. Shen, “Hydrothermal Synthesis of In2O3 for Detecting H2S,” *Sensors Actuators B,* vol. 115, pp. 642 -646, 2006.

[103] Y. L. Liu, H. Wang, Y. Yang, Z. M. Liu, H. F. Yang, G. L. Shen and R. Q. Yu, “Hydrogen Sulphide Sensing Properties of NiFeO4 Nanopowder Doped with Noble Metal,” *Sensors Actuators B,* vol. 102, pp. 148-154, 2004.

[104] D. J. Smith, J. F. Velelina, R. S. Falconer and E. L. Wittman, “Stability Sensitivity and Selectivity of Tungsten Trioxide Films for Sensing Applications,” *Sensors Actuators B,* vol. 13, pp. 264-268, 1993.

[105] W. H. Tao and C. H. Tsai, “H2S Sensing Properties of Noble Metal Doped WO3 Thin Film Sensor Fabricated by Micromachining,” *Sensors Actuators B,* vol. 81, pp. 237-247, 2002.

[106] G. Sberveglieri, S. Groppelli, P. Nelli, C. Perego, G. Valdre and A. Camanzi, “Detection of Sub-ppm H2S Concentrations by SnO2 (Pt) Thin Films Grown by the RGTO Technique,” *Sensors Actuators B,* vol. 55, pp. 86-89, 1998.

[107] Z. L. Wang, “FUNCTIONAL OXIDE NANOBELTS: Materials, Properties and Potential Applications in Nanosystems and Biotechnology,” *Annual Review Physical Chemistry,* vol. 55, p. 159–96, 2004.

[108] M. Parthibavarman, B. Renganatahn and D. Sastikumar, “Development of high sensi-tivity ethanol gas sensor based on Co-doped SnO2nanoparticles by microwaveirradiation technique,” *Current Applied Physics,* vol. 13, p. 1537–1544, 2013.

[109] Y. Wang, Y. Li, C. Rong and J. P. Liu, “Sm–Co hard magnetic nanoparticles prepared by surfactant-assisted ball milling,” *Nanotechnology,* vol. 18, pp. 465701-465704, 2007.

[110] higher, For 8000M-115 and 8000M-230 with Serial Numbers 10115 and; 87011, this manual is Part No..

[111] B. A. Wills, “Mineral Processing Technology, An introduction to the Practical Aspects of Ore Treatment and Mineral Recovery,” *Pergamon Press Oxford,* vol. 07, 2006.

[112] R. Sharma, D.P. Bisen, U. Shukla and B. G. Sharma, “X-ray diffraction: a powerful method of characterizing nanomaterials,” *Recent Research in Science and Technology,* vol. 4(8), pp. 77-79 , 2012.

[113] M. Arshad, A. Azam, A. S. Ahmed, S. Mollah AND A. H. Naqvi, “Effect of Co substitution on the structural and optical properties of ZnO nanoparticles synthesized by sol-gel route,” *Journal of Alloys and Compound,* vol. 509, pp. 8378-8381, 2011.

[114] W. Bekhti, M. Ghamnia and L.Guerbous, “Effect of some amines, dodecylamine (DDA) and hexadecyldimethylamine (DMHA), on the formation of ZnO nanorods synthesized by hydrothermal route,” *Materials Science,* vol. 94, pp. 2886-2899, 2014.

[115] [http://chemwiki.ucdavis.edu/Core/Analytical_Chemistry/Instrumental_Analysis/Diffraction/Powder_X-ray_Diffraction].

[116] J. El Ghoul, C. Barthou and L. El Mir, “Synthesis, structural and optical properties of nanocrystalline vanadium doped zinc oxide aerogel,” *Physica E: Low-dimensional Systems and Nanostructures,* vol. 44, pp. 1910-1915, 2012.

[117] D. E Newbury, P. Echlin, D. C. Joy, A. D. Roming, Jr. C. E. Lyman, C. Fiori and E. Lifshin, Scanning Electron Microscopy and X-ray Microanalysis, New York and London: Plenum Press, 1992.

[118] J. Kwang-Oh and K. Dong-Hwan, “A dither signal imposition to enhance an image in a scanning electron microscope,” *Journal Microelectronic Engineering ,* vol. 88, pp. 2601-2603 , 2011.

[119] [https://www.purdue.edu/ehps/rem/rs/sem.htm].

[120] H. Lim, S. Park, H. Cheong, H.-M. Choi, Y.C. Kim , “Discrimination between natural and HPHT-treated type IIa diamonds using photoluminescence spectroscopy,” *Diamond and Related Materials,* vol. 19, p. 1254–1258, 2010.

[121] C. M. Breeding, A. H. Shen, S. Eaton-Magaña, G. R. Rossman, J. E. Shigley and A. Gilbertson, “Velopments in gemstone analysis techniques and instrumentation during the 2000s,” *G&G,* vol. 46, p. 241–257, 2010.

[122] M.S.Pradeep Kumar Patnaik, K.Rama Kumara Teja and Y.Haritha, “Spectrophotometric determination of organic samples,” *International Journal of Current Engineering and Scientific Research (IJCESR),* vol. 2, pp. 40- 43, 2015.

[123] B. S. Rema Devi, R. Raveendran and A. V. Vaidyan, “Synthesis and characterization of Mn2+-doped ZnS nanoparticles,” *Pramana – Journal of Physics,* vol. 68, p. 679–687, 2007.

[124] J. I. Pankove, Optical process in semiconductors, Prentice-Hall: New Jersey, 1971.

[125] [https://upload.wikimedia.org/wikipedia/commons/archive/9/95/20140312170725%21Schematic_of_UV-_visible_spectrophotometer.png].

[126] F. A. Settle, Handbook of instrumental techniques for analytical chemistry, New Jersey: Prentice, Inc., 1997.

[127] J. M. Chalmers,H. G. M. Edwards and M. D. Hargreaves, Infrared and Raman spectroscopy in forensic science. 1st edition, United Kingdom: John Wiley & Sons Ltd., 2012.

[128] H. H. Willard, Jr L. L. Meritt ,J. J. Dean and Jr F. A. Settle, Instrumental methods of analysis. 7th edition, New Delhi: CBS Publisher & Distributors, 1988.

[129] P. L. Larkin, IR and Raman Spectroscopy: Principles and Spectral Interpretation, USA: Elsevier, 2011.

[130] T. Li, Lie Xu, “A high heating efficiency two beam microplate for catalytic gas sensors,” in *Proceedings of the IEEE International Conference on Micro Electronic and Mechanical Systems MEMS*, Kyoto, Japan, 2012.

[131] Z. Yunusa, M. N. Hamidon, A. Kaiser and Z. Awang, “Gas Sensors: A Review,” *Sensors & Transducers,* vol. 168, pp. 61-75, 2014.

[132] A. Oprea, N. Barsan, U. Weimar, M. Bauersfeld, D. Ebling and J. Wollenstein, “Capacitive humidity sensors on flexible RFID labels,” *Sensors and Actuators B,* vol. 132, p. 404–410 , 2008.

[133] M.-L. Bauersfeld, “Semiconductor gas sensors using thin and thick film technology,” *Fraunhofer Institute for Physical Measurement Techniques IPM,* pp. 1-2.

[134] M. L. Bauersfeld, P. Neumaier and J. Wöllenstein, “Nanoporous Tungsten Trioxide Grown by Electrochemical Anodization of Tungsten for Gas Sensing Applications,” *Procedia Engineering,* vol. 47, pp. 204 - 207, 2012.

[135] G. Rani and P. D. Sahare, “Structural and Spectroscopic Characterizations of ZnO Quantum Dots Annealed at Different Temperatures,” *Journal of Material Science and Technology,* vol. 29, pp. 1035-1039, 2013.

[136] T. N. Soitah, Y. Chunhui and S. Liang, “Effect of Fe doping on structural and electrical properties of nanocrystalline ZnO thin films prepared by sol–gel dip coating technique,” *Science of Advanced Materials,* vol. 2, p. 534–538, 2010.

[137] H. Kind, H. Q. Yan, B. Messer, M. Law and P. D. Yang, “Nanowire ultraviolet photodetectors and optical switches,” *Advanced Materials,* vol. 14, p. 158–160, 2002.

[138] A. Chakraborty, T. Mondal, S. K. Bera, S. K. Sen, R. Ghosh and G. K. Paul , “Effects of Al and In incorporation on the structural and optical properties of ZnO thin films synthesized by spray pyrolysis technique,” *Materials Chemistry and Physics,* vol. 112, pp. 162-168, 2008.

[139] Y. Li, C. Cheng, X. Dong, J. Gao and H. Zhang , “Facile fabrication of UV photodetectors based on ZnO nanorod networks across trenched electrodes,” *Journal of Semiconductors,* vol. 30, p. 38–41, 2009.

[140] I. Djerdj, Z. Jaglicic, D. Arcon and M. Niederberger, “Co-Doped ZnO nanoparticles: Minireview,” *Nanoscale,* vol. 2, p. 1096–1104, 2010.

[141] M. L. Dinesha, H. S. Jayanna, S. Mohanty and S. Ravi, “Structural, electrical and magnetic properties of Co and Fe co-doped ZnO nanoparticles prepared by solution combustion method,” *Journal of Alloys and Compounds,* vol. 490, p. 618–623, 2010.

[142] J. N´emeth, G. Rodriguez-Gattorno, D. Diaz, A.R. V´azquez-Olmos and I. D´ek´any, “Synthesis of ZnO nanoparticles on a clay mineral surface in dimethyl sulfoxide medium,” *Langmuir,* vol. 20, p. 2855–2860, 2004.

[143] L. Spanhel and M. A. Anderson, “Semiconductor clusters in the sol–gel process: quantized aggregation, gelation, and crystal growth a concentrated ZnO colloids,” *J. Am. Chem. Soc.,* vol. 113, p. 2826–2833, 1991.

[144] D. W. Bahnemann, C. Kormann and M. R. Hoffmann, “Preparation and characterization of quamntum size zinc oxide: a detailed specroscopic study,” *Journal of Physical Chemistry,* vol. 91, p. 3789–3798, 1987.

[145] M. W. Maswanganye, K. E. Rammutla, T. E. Mosuang, B. W. Mwakikunga, S. T. Bertrand and M. Maaza,, “The influence of incorporating cobalt (Co) and indium (In) co-dopants on the structural and optical properties of ZnO nanoparticles,” *Advanced Materials Letters,* vol. 8(1), pp. 37- 41, 2017.

[146] J. Liu, T. Luo, F. Meng, K. Qian, Y. Wan and J. Liu, “Porous Hierarchical In2O3 Micro-/Nanostructures: Preparation, Formation Mechanism, and Their

Application in Gas Sensors for Noxious Volatile Organic Compound Detection," *Physical Chemistry C,* vol. 114, p. 4887–4894, 2010.

[147] R. Shannon, "Revised effective ionic radii and systematic studies of interatomic distances in halides and chalcogenides," *Acta Crystallographica Section A,* vol. 32, pp. 751-767, 1976.

[148] Y. Zhang, J. Mu, "Controllable synthesis of flower-and rod-like ZnO nanostructures by simply tuning the ratio of sodium hydroxide to zinc acetate," *Nanotechnology,* vol. 18, p. 075606, 2007.

[149] A. K. Zak, W. H. A. Majid, M. E. Abrishami, R. Yousefi, "X-ray analysis of ZnO nanoparticles by Williamson-Hall and size-strain plot method," *Solid State Sciences,* vol. 13, pp. 251-256, 2011.

[150] Z. Fan, J. G. Lu, "Zinc oxide nanostructures: synthesis and properties," *Nanoscience Nanotechnology,* vol. 5, p. 1561–1573, 2005.

[151] K. Shingange, G. H. Mhlongo, D. E. Motaung and O. M. Ntwaeaborwa, "Tailoring the sensing properties of microwave-assisted grown ZnO nanorods: Effect of irradiation time on luminescence and magnetic behaviour.," *Journal of Alloys and Compounds,* vol. 657, pp. 917-926, 2016.

[152] G. H. Mhlongo, D. E. Motaung, S. S. Nkosi, H. C. Swart, G. F. Malgas, K. T. Hollie, B. W. Mwakikunga, "Temperature dependence on the structural, optical, and paramagnetic properties of ZnO nanostructures," *Applied Surface Science,* vol. 293, pp. 62-70, 2014.

[153] T. C. Damen, S. P. S. Porto, B. Tell, “Raman Effect in Zinc Oxide,” *Physical Review,* vol. 142, pp. 570-574, 1966.

[154] S. K. Panda, C. Jacob, “Surface enhanced Raman scattering and photoluminescence properties of catalytic grown ZnO nanostructures,” *Applied physics A,* vol. 96, pp. 805-811, 2009.

[155] Y. Wang, X. Li, N. Wang, X. Quan, Y. Chen,, “Controllable synthesis of ZnO nanoflowers and their morphology-dependent photocatalytic activities,” *Sep. Purif. Technol,* vol. 62, pp. 727-732, 2008.

[156] A. Khan, “Raman Spectroscopic Study of the ZnO Nanostructures,” *Journal of Pakistan Materials Society,* vol. 4(1) , pp. 5-9, 2010.

[157] M. Schumm, J. Geurts, R. Neder,, “ZnO-based semiconductors studied by Raman spectroscopy: semimagnetic alloying, doping, and nanostructures,” 2009.

[158] G. L. Kabongo,G. H. Mhlongo, T. Malwela, B. M. Mothudi, K. T. Hillie, M. S. Dhlamini,, “Microstructural and photoluminescence properties of sol-gel derived Tb3+ doped ZnO nanocrystals,” *Journal of Alloys Compound,* vol. 591, pp. 156-163, 2014.

[159] C. Wang, E. Shen, E. Wang, L. Gao, Z. Kang, C. Tian, Y. Lan C. Zhang, “Controllable synthesis of ZnO nanocrystals via a surfactant-assisted alcohol thermal process at a low temperature,” *Materials Letters,* vol. 59, pp. 2867-2871, 2005.

[160] J. Chen, J. Li, G. Xiao, X. Yang, “Large-scale syntheses of uniform ZnO nanorods and ethanol gas sensors application,” *Journal of Alloys Compound,* vol. 509, p. 740–743, 2011.

[161] D. E. Motaung, P. R. Makgwane, S. S. Ray,, “Induced ferromagnetic and gas sensing properties in ZnO-nanostructures by altering defect concentration of oxygen and zinc vacancies,” *Materials Letters,* vol. 139, p. 475–479, 2015.

[162] M. Willander, O. Nur, J. R. Sadaf, M. I. Qadir, S. Zaman, A. Zainelabdin, N. Bano, I. Hussain, “Luminescence from Zinc Oxide Nanoprticles and Polymers and their Hybrid Devices,” *Materials,* vol. 3, pp. 2643-2667, 2010.

[163] Z. Yunusa, M. N. Hamidon, A. Kaiser and Z. Awang, “Gas sensors: A review,” *Sensors and transducers,* vol. 168, pp. 61-75, 2014.

[164] J. H. Yu, G. M. Choi, “Electrical and CO Gas Sensing Properties of ZnO-SnO2 Composites,” *Sensors and Actuators B,* vol. 52, p. 251–256, 1998.

[165] D. H. Yoon, J. H. Yu and G. M. Choi, “CO Gas Sensing Properties of ZnO-CuO,” *Composites Sensors and Actuators B,* vol. 46, pp. 15-23, 1998.

[166] C. L. Zhu, Y. J. Chen, R. X. Wang, L. J. Wang, M. S. Cao, X. L. Shi, “Synthesis and Enhanced Ethanol Sensing Properties of α-Fe2O3/ZnO Heteronanostructures.,” *Sensors and Actuators B,* vol. 140, p. 185–189, 2009.

[167] W. Göpel and K. D. Schierbaum, “SnO2 Sensors-Current Status and Future Prospects,” *Sensors and Actuators B,* vol. 26, pp. 1-12, 1995.

[168] P. Feng,Q. Wan and T. H. Wang, “Contact-controlled sensing properties of flowerlike ZnO nanostructures,” *Applied Physics Letters,* vol. 87, p. 213111, 2005.

[169] J. Tamaki, T. Maekawa, N. Miura and N. Yamazoe, “CuO-SnO 2 element for highly sensitive and selective detection of H2S,” *Sensors and Actuators B,* vol. 9, pp. 197-203, 1992.

[170] C. Wang, L. Yin, L. Zhang, D. Xiang and R. Gao, “Metal Oxide Gas Sensors: Sensitivity and Influencing Factors,” *Sensors,* vol. 10, pp. 2088-2106, 2010.

[171] T. Maekawa, J. Tamaki, N. Miura and N. Yamazoe, “Sensing behaviour of CuO loaded SnO2 element for H2S detection,” *Chem. Left.,* vol. 1991, pp. 575-578, 1991.

[172] V. Lantto and P. Romppainen, “Response of some SnO2 gas sensors to H2S after quick cooling,” *Journal of Electrochemical Society,* vol. 135, pp. 2550-2556, 1988.

[173] J. Lui, X. Huang, G. Ye, W. Lui, Z. Jiao, W. Chao, Z. Zhou and Z. Yu, “H2O detection sensing characteristic of CuO/SnO2 sensor,” *Sensor,* vol. 3, pp. 110-118, 2003.

[174] K. Qin, L. Chang-Shi, L. Zhou, L. Yu-Zi, X. Zhao-Xiong, Z. Lan-Sun and L. W. Zhong, “Enhancing the Photon- and Gas-Sensing Properties of a Single SnO2 Nanowire Based Nanodevice by Nanoparticle Surface Functionalization,” *Journal of Physical Chemistry C,* vol. 112, p. 11539–11544, 2008.

[175] J. X. Wang, X. W. Sun, Y. Yang, H. Huang, Y. C. Lee, O. K. Tan and L. Vayssieres, “Hydrothermally grown oriented ZnO nanorod arrays for gas sensing applications,” *Nanotechnology,* vol. 17, p. 4995–4998, 2006.

[176] A. Karthigeyan, R.P. Gupta, M. Burgmair , S.K. Sharma, “Influence of oxidation temperature, film thickness and substrate on NO2 sensing of SnO2 ultra thin films,” *Sensors and Actuators B,* vol. 87, p. 321–330, 2002.

[177] M. Joseph, H. Tabata and T. Kawai, “n-type electrical conduction in ZnO thin films by Ga and N Codoping,” *Japanese Journal of Applied Physics,* vol. 38, pp. L 1205-L 1207, 1999.

[178] Y. J. Chen, X. Y. Xue, Y. G. Wang and T. H. Wang, *Applied Physics Letters,* vol. 87, pp. 233503-233505, 2005.

[179] M. Acuautla, S. Bernardini, M. Bendahan and L. Gallais, “Ammonia sensing properties of ZnO nanoparticles on flexible substrate,” in *Proceedings of the 8th International Conference on Sensing Technology, Sep. 2-4*, Liverpool, UK, 2014.

[180] D. A. Stolper, M. Lawson, C. L. Davis, A. A. Ferreira, E. V. Santos Neto, G. S. Ellis, M. D. Lewan, A. M. Martini, Y. Tang, M. Schoell, A. L. Sessions and J. M. Eiler , “Gas formation. Formation temperatures of thermogenic and biogenic methane,” *Science,* vol. 344, pp. 1500-1503, 2014.

[181] D. E. Motaung, P. R. Makgwane and S. S. Ray, “Induced ferromagnetic and gas sensing properties in ZnO-nanostructures by altering defect

concentration of oxygen and zinc vacancies," *Materials Letters,* vol. 139, pp. 475-479, 2015.

[182] W. Hyung-Sik, k. Chang-Hoon, k. Il-Doo, and L. Jong-Heun , "Selective, sensitive, and reversible detection of H2S using Mo-doped ZnO nanowire network sensors," *Materials Chemistry A,* vol. 2, pp. 6412-6418, 2014.

[183] W. Zang, Y. Nie, D. Zhu, P. Deng, L. Xing and X. Xue, "Core−Shell In2O3/ZnO Nanoarray Nanogenerator as a Self-Powered Active Gas Sensor with High H2S Sensitivity and Selectivity at Room Temperature," *Journal of Physical Chemistry C,* vol. 118, p. 9209−9216, 2014.

[184] Z. Zeng, K. Wang, Z. Zhang, J. Chen and W. Zhou, "The detection of H2S at room temperature by using individual indium oxide nanowire transistors," *Nanotechnology,* vol. 20, p. 045503 (4pp), 2009.

[185] T. V. Cuong, V. H. Pham, J. S. Chung, E. W. Shin, D. H. Yoo, S. H. Hahn, J. S. Huh, G. H. Rue, E. J. Kim, S. H. Hur and P. A. Kohl, "Solution-processed ZnO-chemically converted graphene gas sensor," *Materials Letters,* vol. 64, p. 2479–2482, 2010.

8. Publications and conference presentations

8.1 Publications

8.1.1 Manamela M.F, Mosuang T.E and Mwakikunga B.W "*The structural and sensing properties of cobalt and indium doped zinc oxide nanopowders synthesised through high energy ball milling technique*." The 62nd annual conference of the South African Institute of Physics (SAIP2017), held at Stellenbosch University, Cape Town, South Africa, 03 - 07 July 2017 (*paper submitted*).

8.1.2 Manamela M.F, Mosuang T.E and Mwakikunga B.W "*Structural and optical property changes of zinc oxide nanopowders doped with cobalt and indium metals mechano-chemically*." Advanced materials proceedings (*paper accepted*).

8.2 Conference presentations

8.2.1 Manamela M.F, Mosuang T.E and Mwakikunga B.W "*The structural and sensing properties of cobalt and indium doped zinc oxide nanopowders synthesised through high energy ball milling technique*." The 62nd annual conference of the South African Institute of Physics (SAIP2017), held at Stellenbosch University, Cape Town, South Africa, 03 - 07 July 2017.

8.2.2 Manamela M.F, Mosuang T.E and Mwakikunga B.W "*Structural and optical studies of mechano-chemically prepared zinc oxide nanopowders co-doped with indium and cobalt*." Faculty of Science and Agriculture Research Day, held at Bolivia Lodge, Polokwane, 24 - 25 October 2016.

8.2.3 Manamela M.F, Mosuang T.E and Mwakikunga B.W "*Structural and optical studies of cobalt and indium simultaneously doped zinc oxide nanopowders prepared using high energy ball milling technique*." The 61st annual conference

of the South African Institute of Physics (SAIP2016), held at University of Cape Town, Cape Town, South Africa, 04-08 July 2016.

8.2.4 Manamela M.F, Mosuang T.E and Mwakikunga B.W "*Synthesis and characterisation of mechano-chemically synthesised zinc oxide nanoparticles using ball milling*". DST-NRF Internship Programme Research Presentation Day 2015/16 held at OR Tambo 19 February 2016.

8.2.5 Manamela M.F, Rammutla K.E and Mosuang T.E, "*Structural and optical studies of cobalt (Co) and indium (In) co-doped zinc oxide nanoparticles prepared using ball milling method*." Faculty of Science and Agriculture Research Day, held at Bolivia Lodge, Polokwane, 01 - 02 October 2015.